

Simulations of normal spiral galaxies

Roelof Bottema

Kapteyn Astronomical Institute, P.O. Box 800, NL-9700 AV Groningen, The Netherlands, e-mail:robot@astro.rug.nl

31 October 2018

ABSTRACT

Results are presented of numerical simulations of normal isolated late type spiral galaxies. Specifically the galaxy NGC 628 is used as a template. The method employs a TREESPH code including stellar particles, gas particles, cooling and heating of the gas, star formation according to a Jeans criterion, and Supernova feedback. A regular spiral disc can be generated as an equilibrium situation of two opposing actions. On the one hand cooling and dissipation of the gas, on the other hand gas heating by the FUV field of young stars and SN mechanical forcing. The disc exhibits small and medium scale spiral structure of which the multiplicity increases as a function of radius. The theory of swing amplification can explain, both qualitatively and quantitatively, the emerging spiral structure. In addition, swing amplification predicts that the existence of a grand design $m = 2$ spiral is only possible if the disc is massive. The simulations show that the galaxy is then unstable to bar formation, confirming the result of Ostriker & Peebles (1973). The occurrence of this bar instability is further investigated. A general criterion is derived for the transition between bar stable and unstable, depending on disc mass contribution and on disc thickness. It seems that bar stability hardly depends on the presence of gas. A detailed quantitative analysis is made of the emerging spiral structure and a comparison is made with observations. That demonstrates that the structure of the numerical isolated galaxies is not as strong and has a larger multiplicity compared to the structure of some exemplary real galaxies. It is argued that the suggestion of Kormendy & Norman (1979) holds, that a grand design can only be generated by a central bar or by tidal forces resulting from an encounter with another galaxy.

Key words: galaxies: evolution – galaxies: general – galaxies: fundamental parameters – galaxies: kinematics and dynamics – galaxies: structure

1 INTRODUCTION

It is now well established that substantial amounts of dark matter are needed to explain flat rotation curves in the outer regions of spiral galaxies. However, the amount of dark matter present in the inner, luminous region of a galaxy is not well determined. Does a spiral galaxy conform to the maximum disc hypothesis (van Albada & Sancisi 1986; Salucci et al. 1991; Sellwood & Moore 1999) which states that the luminous part should be scaled up as much as possible? Or is the maximum rotational contribution of the disc to the total rotation around 63%? The latter being derived from observations of disc stellar velocity dispersions (Bottema 1993, 1997) or suggested by a statistical analysis of rotation curve shapes in relation to the compactness of discs (Courteau & Rix 1999). When discs obey the 63% criterion, their mass-to-light ratio is half that of the maximum disc case, but the disc still dominates in the inner two to three scalelengths. A rotation curve analysis generally allows a maximum disc rotational contribution anywhere between 50 to 90% (van

der Kruit 1995). The above mentioned velocity dispersion measurements have only been done for a dozen galaxies and the analysis depends on the not well determined ratio of disc scalelength to scaleheight. As observations are not yet conclusive, numerical simulations of spiral galaxies may give clues regarding the disc to halo mass ratio.

Spiral structure of galaxies has eluded astronomers already for a long time. Is it a quasi stationary density wave (Lin & Shu 1964, 1966)? Or is it a temporal phenomenon excited by internal or external disturbances and then swing amplified (Goldreich & Lynden-Bell 1965; Toomre 1981)? Or is it some kind of combination, like swing amplified density waves? Until now theory and observations are inconclusive. To compound matters, there is the “anti spiral theorem” (Lynden-Bell & Ostriker 1967), which states that spiral structure cannot develop in a system governed by a time reversible description. Consequently spiral arms cannot exist in an isolated pure stellar galaxy. Some kind of non time reversible action is needed, like external forcing or gas dissipation. The need for the latter mechanism is confirmed

observationally; in general when there is no gas there are no spiral arms. When studying spiral structure one thus has to include a gaseous component in the calculations. Doing that, calculations in three dimensions are required because for a typical disc the scaleheight of the stellar component is five times as large as the scaleheight of the gas layer.

Some galaxies have bars, others don't. Ostriker & Peebles (1973) showed that a stellar disc can be stabilized against bar formation by adding a spherical (dark halo) potential. This has led to the common belief that barred galaxies have a larger disc to halo mass ratio compared to non-barred galaxies, although there is no observational evidence to support this belief. Other theoretical and numerical calculations (Efstathiou et al. 1982; Bottema & Gerritsen 1997) investigating this matter reconfirm that a relatively larger disc mass results in a galaxy which is more unstable to bars. Therefore this ratio is inevitably an important parameter in determining the appearance of a galaxy. Another effective parameter has to be the stellar velocity dispersion of a disc. Larger dispersions, expressed in a larger Toomre's (1964) Q value, lead to a more stable disc (Sellwood & Carlberg 1984). In addition a substantial bulge makes a disc more stable against bars (Sellwood & Evans 2001).

A proper investigation of disc galaxies involves a.o. dissipational and non linear processes. Therefore this subject is not easily handled by analytical calculations and one has to resort to numerical simulations. Results of such simulations can then guide the way to more detailed analyses of some specific aspects. Concerning numerical simulations, the combination of the tree code (Barnes & Hut 1986) for the collisionless part of a galaxy with the Smoothed Particle Hydrodynamics (SPH) algorithm (Lucy 1977) for the collisional part allows the study of a galaxy containing gas. However, this combined TREESPH code (Hernquist & Katz 1989) has rarely been used to study the detailed evolution and stability of isolated galaxies. It has mainly been applied to investigate interacting galaxies (Barnes & Hernquist 1991; Mihos & Hernquist 1994; Springel 2000), galaxy formation (Katz & Gunn 1991; Katz 1992) or barred galaxies specifically (Friedli & Benz 1993, 1995). A preliminary numerical study of spiral structure has been performed by Elmegreen & Thomasson (1993) while Gerritsen (1997) and Gerritsen & Icke (1997, hereafter: GI97) made a detailed numerical analysis of the distribution and interaction of the stellar and gaseous components in an isolated galaxy.

For a galaxy simulation one needs at least stars and gas. An optional bulge can be added and in order to make the observed flat rotation curves, a dark halo should be included. When gas is present, that cools and dissipates so that a star formation (SF) prescription is needed. That leads to gas depletion and to the formation of young stars with low velocity dispersions. SF also generates heating and stirring of the gas, preventing it from further collapse and so establishing a feedback loop which creates some kind of interstellar gas medium in equilibrium. These processes are too complex to be simulated from basic principles so that one needs a global description for the entities and processes in galaxy simulations.

Concerning SF there is a clear observational result, namely the Schmidt (1959) law which states that the SF rate (SFR) is proportional to the gas density to a power n : $\text{SFR} \propto \rho^n$. Detailed observations and analyses by Kenni-

cutt (1983, 1989, 1998) and by Ryder & Dopita (1994) show that this Schmidt law holds with $n \sim 1.3$ for a wide range of (surface) densities in galactic discs. Consequently this observation and proper exponent has to be the outcome of any numerical SF prescription. The interesting result of GI97 is that they reproduce the right Schmidt law by using a star formation law based on a Jeans criterion. They do not impose the Schmidt law a priori, but it is the result of a more fundamental process. Their scheme is therefore expected to hold for a broad range of physical conditions.

It is well known that in a real galaxy young stars and SF regions exert a definite action on the ambient ISM. The fierce radiation heats the gas and supernova (SN) action stirs up the ensemble of gas clouds. This SF feedback maintains an equilibrium state of the ISM. When simulations lack such a feedback a catastrophic gas cooling occurs, forming super giant cloud complexes (Shlosman & Noguchi 1993). Therefore in the numerical calculations also a SF feedback prescription is needed.

As mentioned above, Elmegreen & Thomasson (1993) made a numerical study of isolated galaxies to specifically investigate spiral structure, more or less as a function of disc to halo mass ratio. They find for a "rather massive" disc a grand design $m = 2$ structure which lasts for several rotation periods. For substantially less massive discs the spiral structure becomes flocculent. Though their investigation is very interesting it contains several caveats. The main one is that the development of a bar is prevented in at least two ways. Firstly by using an artificial Q barrier in the inner regions. Secondly the disc is stabilized by a large softening length (Romeo 1994) which has to be used to perform the two dimensional simulations. Therefore it is expected that the results of Elmegreen & Thomasson only partially apply to a real galaxy. Results in the present paper differ from the study of Elmegreen & Thomasson mainly relating to the development of a bar in massive discs.

My original intention was to investigate what happens to the morphology of a normal galaxy when the ratio of disc to dark matter changes. Inevitably, during the research other and additional problems emerged which necessitated a somewhat broader scope. Nevertheless this paper still focuses on the global properties and global morphology of a galaxy and does not aim to go into specific details. Besides the abovementioned mass ratio another defining parameter for a galactic disc is the value of the stellar velocity dispersion, or more or less equivalently, the thickness of the disc. In addition effects of the amount of SN feedback and amount of available gas have been considered. The investigations are restricted to late type galaxies for which NGC 628 serves as template. That galaxy is nearly face-on, has only a minor bulge, and has a well defined, non barred spiral structure.

Section 2 of this paper describes the code and all the relevant prescriptions. The employed numerical scheme is based on the works of GI97, Gerritsen (1997), and Hernquist & Katz (1989). Besides the nice asset of reproducing the Schmidt law, the scheme creates a multiple phase interstellar medium, equal to the situation in a real galaxy. GI97 performed their simulations for galaxies with low SF rates and then an equilibrium gas state can be achieved by UV heating only. When the SFR crosses a certain threshold it is necessary to include mechanical feedback in addition. This supernova feedback will be described in sufficient de-

tail. In Sect. 3 the model galaxy is described and in Sect. 4 several properties and adaptations are discussed. To create a realistic disc in star formation equilibrium in Sect. 5 the necessary amount of SN feedback and external gas supply are determined. Section 6 describes what happens when the main parameters; disc to halo mass ratio and disc thickness are varied. When does a bar form and what is the global morphology? In Sect. 7 an analysis and discussion is given of the gas properties, like temperature distribution and gas velocity dispersion. Section 8 deals in some detail with the spiral structure and compares results from the simulations with observations. In Sect. 9 the theory of swing amplification is applied to the galaxies under investigation and finally in Sect. 10 a general discussion is given and a point by point summary of the conclusions.

2 THE CODE

2.1 Numerical technique

The evolution of a galaxy is simulated using a hybrid N-body/hydrodynamics code (TREESPH; Hernquist & Katz 1989). A tree algorithm (Barnes & Hut 1986; Hernquist 1987) determines the gravitational forces on both the stellar and gaseous components of the galaxy. The hydrodynamic properties of the gas are modelled using the method of smoothed particle hydrodynamics (Lucy 1977; Gingold & Monaghan 1977). The gas evolves according to hydrodynamic conservation laws, including an artificial viscosity for the treatment of shocks. Each gas particle is assigned an individual smoothing length, h_i , which determines the local resolution. Gas properties are found by smoothing over N neighbours within $2h$, where N is typically 64 for a number of gas particles larger than 12,000. The acceleration (\vec{a}_i) of particle i is given by

$$\vec{a}_i = -\frac{1}{\rho_i} \nabla P_i + \vec{a}_i^{\text{visc}} - \nabla \Phi_i, \quad (1)$$

with P being the pressure, \vec{a}_i^{visc} the artificial viscosity term (Monaghan 1989), and Φ the gravitational potential. For the evolution of the specific thermal energy (u) an expression is chosen as

$$\frac{du_i}{dt} = \frac{1}{2} \vec{v}_i \cdot \left(\frac{1}{\rho_i} \nabla P_i - \vec{a}_i^{\text{visc}} \right) + \frac{\Gamma - \Lambda}{\rho}, \quad (2)$$

where $(\Gamma - \Lambda)/\rho$ accounts for the non-adiabatic heating and cooling terms. To close the system of equations describing the evolution of the fluid an equation of state

$$P = (\gamma - 1)\rho u, \quad (3)$$

is adopted with $\gamma = 5/3$ for an ideal gas.

Time steps of the stellar particles were equal to $1.5 \cdot 10^6$ years. For gas (SPH) particles a variable time step was used determined by the Courant-Friedrichs-Levy condition, with a maximum of $1.5 \cdot 10^6$ years. The softening of stellar particles was not implemented by the usual softened force law: $a \propto (r^2 + \varepsilon^2)^{-1}$ but by a smoothing kernel surrounding the stellar particle (Hernquist & Katz 1989). In that way a better approximation is achieved of the real force law.

2.2 The cooling

The cooling term Λ in Eq. (2) describes the radiative cooling of the gas. For the simulations a constant composition of H I plus Helium gas is adopted. The “standard” cooling function of Dalgarno & McCray (1972) was used for this gas, parameterized as

$$\frac{\Lambda}{[\text{erg cm}^{-3} \text{ s}^{-1}]} = 10^{-21} n_H^2 \left[10^{-0.1-1.88(5.23-\log T)^4} + 10^{-a-b(4-\log T)^c} \right] \text{ if } \log T < 6.2 \quad (4)$$

and

$$\frac{\Lambda}{[\text{erg cm}^{-3} \text{ s}^{-1}]} = 10^{-22.7} n_H^2 \text{ if } \log T > 6.2, \quad (5)$$

where T is the temperature and n_H the hydrogen density in cm^{-3} . The second term on the right hand side of Eq. (4) determines the cooling below 10^4 K, which is strongly dependent on the amount of ionization of the H I gas. For an ionization parameter n_e/n_H of 0.1 (Cox 1990) a good approximation of Dalgarno & McCray’s cooling function is found for $a = 3.24$, $b = 0.085$, and $c = 3.0$.

The star formation rate is dependent on the amount of cooling below 10^4 K and the parameter a mainly determines this amount. For a lower ionization or for lower abundances the cooling will be smaller and the SFR lower (Gerritsen & de Blok 1999). In the calculations the cooling rate for all gas is set a priori equal to approximately the solar neighbourhood value. The effects of metallicity changes in a galaxy have not been considered.

2.3 Heating

The heating of the gas (Γ) is described by two terms:

$$\frac{\Gamma}{[\text{erg s}^{-1} \text{ cm}^{-3}]} = 10^{-24} \epsilon G_0 n_H + C_{\text{cr}} n_H, \quad (6)$$

where the first term represents photoelectric heating of small grains and PAHs (de Jong 1977; Wolfire et al. 1995) and dominates in the stellar disc region. In Eq. (6) ϵ is the heating efficiency and G_0 is the incident far-ultraviolet field (912 to 2100 Å) normalized to Habing’s (1968) estimate of the local interstellar value ($= 1.6 \cdot 10^{-3} \text{ erg cm}^{-2} \text{ s}^{-1}$). This heating efficiency $\epsilon \approx 0.05$ for temperatures below 10,000 K. The second term in Eq. (6) represents the so called “cosmic ray” heating (Black 1987; Spitzer 1978). A value of $7.8 \cdot 10^{-27} \text{ erg s}^{-1}$ has been used for the cosmic ray heating constant C_{cr} . In a normal stellar environment cosmic ray heating is negligible compared to the grain heating. Yet in the outer regions of a galaxy, beyond the stellar edge, it is still small, but it is the only heating source. This term has been included after the work of GI97 to prevent too much cooling and star formation in those outer regions.

Since the gas is heated mainly by FUV photons, the stellar radiation field has to be calculated. In the simulations each stellar particle effectively represents a stellar association. Such an association is formed instantaneously and consequently each stellar particle has an age and a belonging FUV flux according to that age. This flux has been calculated using the population synthesis models of Bruzual & Charlot (1993) for a certain specified IMF. Knowing the

FUV flux for every stellar particle, the radiation field is calculated by summing the individual fluxes corrected for geometric dilution. No extinction corrections have been applied. The cooling of the gas increases by more than a factor 10^3 for temperatures rising above 10^4 K. That temperature is therefore effectively an upper limit, virtually independent of the heat input.

2.4 The star formation criterion

Star formation on scales \lesssim giant molecular clouds is a very complicated process. It involves matters like heating/cooling balance, collapse, fractionization and sub fractionization, the transition of H I into H₂, magnetic fields, winds, SN explosions, shocks, ionization, desintegration, etc, etc. GMCs, where the star formation takes place, have typical masses of a few times 10^5 to $10^6 M_\odot$, densities $> 10^3 \text{ cm}^{-3}$ and lifetimes of 10^7 to 10^8 years (Shu et al. 1987; Bodenheimer 1992). Masses of gas particles in the simulation range typically from $5 \cdot 10^5$ to 10^6 solar masses, being comparable to GMCs. A star formation recipe is thus a prescription of converting GMCs into stellar associations and does not consider all the processes mentioned above.

The formation of stellar associations (\equiv stellar particles) proceeds nearly equal as described by GI97. For convenience a summary of this star formation process will be given. In SPH simulations the gas particles sample properties such as density and temperature. For each particle one can therefore calculate the Jeans mass M_J

$$M_J = \frac{1}{6} \pi \rho \left(\frac{\pi c_s^2}{G \rho} \right)^{3/2}, \quad (7)$$

where ρ is the density, c_s the sound speed and G the gravitational constant. If this Jeans mass is smaller than a prescribed critical mass M_{crit} , which is of the order of the mass of a GMC, then the gas particle is in a cold and dense environment and is considered unstable to star formation. So, the condition $M_J < M_{\text{crit}}$ is a first criterion a gas particle has to obey to form a stellar particle.

Once a region is unstable, it takes a collapse time to form a stellar cluster. As a second criterion it has been chosen that a gas particle has to remain unstable for a time span longer than a fraction f_c of the free-fall time t_{ff} :

$$t_{\text{span}} > f_c \times t_{\text{ff}} = \frac{f_c}{\sqrt{4\pi G \rho}}. \quad (8)$$

As soon as an SPH particle has fulfilled both conditions (7) and (8) a part of its mass (M_g) is converted into a stellar particle with mass M_*

$$M_* = \epsilon_{\text{sf}} \times M_g. \quad (9)$$

This continues until the mass of a gas particle would drop below 0.1 times its original mass, then the whole remaining gas particle is turned into a new star. The star particle is given the same IMF as all other star particles, and age zero. New star particles are then included in the calculation of the radiation field and the ambient gas will be heated. In this way a self regulating star formation process is established.

GI97 made a thorough investigation of the effects when a specified SF parameter is changed. In short, the cooling function essentially determines the SFR and a change of the

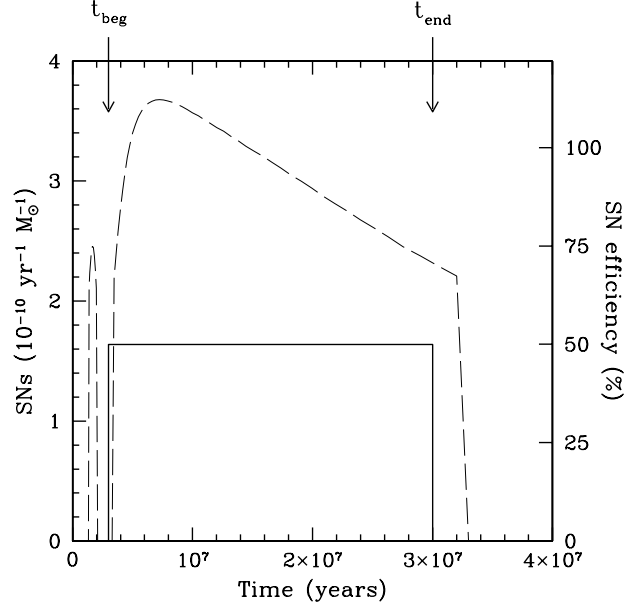


Figure 1. Graphical representation of supernova (SN) feedback. The dashed line and left axis give the number of SNs as a function of time following Bruzual and Charlot (1993). In the code the mechanical SN feedback is implemented by giving a certain fraction (SN efficiency) of the belonging SN energy as a constant thermal energy to one SN particle. This is illustrated by full drawn line and right axis for a SN action from $t = t_{\text{beg}}$ to $t = t_{\text{end}}$ for $\epsilon_{\text{SN}} = 50\%$.

collapse factor f_c changes the ratio of warm to cold gas. Changing other parameters has a negligible or only a small effect on observable structures and quantities. In the present study the star formation parameters are essentially fixed at a certain value. The critical mass M_{crit} is equal to the value of a GMC, the IMF is Salpeter ($0.1 \rightarrow 125 M_\odot$), the cooling function is solar neighbourhood and $\epsilon_{\text{sf}} = 0.5$. The collapse factor was determined at 0.5 such that the gas is not too clumpy and the warm to cold gas ratio is reasonable (see Sect. 5.1 and 7.2).

2.5 Supernova feedback

Besides the FUV feedback on the gaseous medium there is also the mechanical feedback by supernovae and stellar winds. A method to implement that feedback has been developed by Gerritsen (1997) which I have largely taken over. Since a description has not appeared in the refereed literature and because a number of changes have been made to the method, a detailed description now follows.

Winds and supernovae from OB associations are capable of blowing cavities in the surrounding ISM. In the standard model for such a process the mechanical energy is injected into a hot bubble which sweeps up the external medium by a dense shell (McCray & Kafatos 1987). Not all the energy is converted into kinetic energy of the expanding shell. Silich et al. (1996) demonstrate that most of the energy is simply radiated away and only 5 to 10% ends up in the expanding shell. An amount of $\sim 10^{51}$ ergs of energy is provided by each supernova so that every star more massive

than $8 M_{\odot}$ supplies that amount to the mechanical feedback process. Additional energy is provided by winds from massive and medium size stars (Lamers & Leitherer 1993).

The more classical implementation of mechanical feedback is by “kicking” the surrounding ISM. The gas around a young star cluster is then given a velocity perturbation directed radially away from the cluster. A free parameter in this implementation is the fraction of the released energy (f_v) that is put into the velocity perturbation. The feedback may have profound effects on the gas depending largely on the value of f_v . For example, Navarro & White (1993) favour values of $f_v \lesssim 0.1$ in their cosmological simulations. But Friedly & Benz (1995) take of the order of 0.01 for barred galaxies and Mihos & Hernquist (1994, 1996) use $f_v \sim 10^{-4}$ for simulations of interacting galaxies. Clearly there is a lot of arbitrariness as to the choice of f_v .

At present a different approach to implement mechanical feedback has been chosen. Following an idea by Heller & Shlosman (1994) a fraction of the mechanical energy is given as thermal energy to one gas particle during a certain amount of time. In this way a hot bubble is simulated by making one SPH particle hot; from now on called SN particle. It is further left to the TREESPH program to distribute the energy to the surrounding gas particles like a pseudo-point explosion.

For the implementation in the code it has to be realized that one is dealing with particles representing GMCs and whole star forming regions. When a gas particle (GMC) is deemed to form a star particle (SF region) half of its mass is transformed into a star particle with zero age and belonging IMF. The other half of the gas particle is designated as SN particle possessing the mechanical energy appropriate for the SF region. For a period of $\sim 3 \cdot 10^7$ years SN activity is present in the SF region and for such a time the SN particle is both, fixed to the parent star particle, and kept hot. To illustrate matters, in Fig. 1 the SN energy is given as a function of time according to the Bruzual & Charlot population synthesis code. On top of that figure the simplified SN particle energy is displayed. For a small time span after star formation SN activity is not yet switched on and the SN particle is kept at a temperature of 10^4 K. After that a fraction ε_{SN} of the total SN energy of the SF region is given as thermal energy to the SN particle. This total SN energy is calculated from the total mass of the new star cluster, the assumed IMF, and the fact that all stars go SN for a mass $> 8 M_{\odot}$. After a time $t_{\text{SN}}^{\text{end}}$ no more energy is supplied to the SN particle and it is allowed to cool again which it will do quickly in practice.

In reality there is a time variability of the SN action (Fig. 1) and a poorly known energy contribution from winds. These details and uncertainties have been included in the free parameter ε_{SN} . After the SN phase the gas particle returns to being a normal SPH particle which may undergo a next event of star formation if the conditions are right. Most simulations in this paper are performed for $\varepsilon_{\text{SN}} = 25\%$, and for a regular SF where half the gas mass is transformed into stars, the belonging temperature of the SN particle amounts to $1.25 \cdot 10^7$ K. In this, albeit artificial, way a three phase ISM is created containing cold, warm, and hot gas (McKee & Ostriker 1977).

Gerritsen (1997) did some testing of this method on isolated galaxies. It appeared that realistic cavities are created

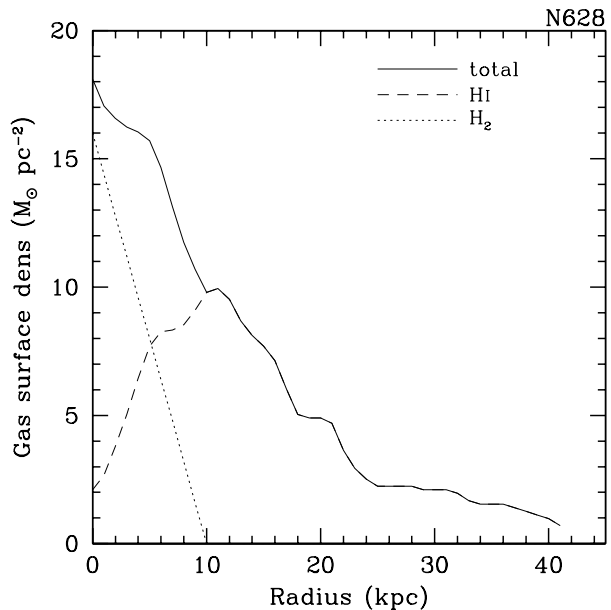


Figure 2. The total gas surface density of NGC 628 which has been used in the model galaxy. H I and H₂ have been added and multiplied by 1.4 to account for Helium.

in the ISM, where the holes are smaller in the central denser regions and larger near the rim of the gas distribution. The size and the size distribution of the holes does not depend on the number of gas particles. This demonstrates the reliability of the method and shows it can be used for a large gas density range even at a limited resolution. Compared to a situation with only FUV heating of the gas, adding the mechanical feedback changes the gas appearance to a different and larger design.

3 THE GALAXY

All the calculations have been performed for one model galaxy with different internal compositions. This galaxy consists of four components: a stellar disc, a gas layer, a bulge, and a dark halo. This disc and gas layer are made up of stellar and gas particles while the bulge and halo are implemented as rigid, “dead”, potentials.

An exponential stellar disc is assumed with a locally isothermal z -distribution (van der Kruit & Searle 1981)

$$\rho_d(R, z) = \rho_0^d e^{-R/h} \text{sech}^2\left(\frac{z}{z_0}\right), \quad (10)$$

where h is the scalelength of the disc and z_0 the thickness parameter which was constant as a function of radius. If the disc were isolated the vertical stellar velocity dispersion $\langle v_z^2 \rangle^{1/2}$ depends on the stellar surface density σ_* as

$$\langle v_z^2 \rangle^{1/2} = \sqrt{\pi G z_0 \sigma_*(R)}. \quad (11)$$

In reality adjustments are necessary to this relation because the other galactic components influence the stellar velocity dispersion. For the setup of the galaxy only the gas has been taken into account such that in Eq. (11) $\sigma_*(R)$ is replaced by $\sigma_*(R) + \sigma_{\text{gas}}(R)$. During the initial stages of the simulations the stellar disc still has to settle in the bulge and halo

Table 1. Galaxy parameters

Disc v_{\max} (km s ⁻¹)	Disc mass (10 ⁹ M _⊙)	Disc central surf. dens. (M _⊙ pc ⁻²)	$\langle v_z^2 \rangle_{R=0}^{1/2}$ for $z_0 = 900$ pc (km s ⁻¹)	Disc (M/L _B)	Halo R_{core} (kpc)	Halo v_{\max} (km s ⁻¹)	Bulge mass (10 ⁹ M _⊙)	Bulge central surf. dens. (M _⊙ pc ⁻²)
126	45.5	367	67	2.05	3	185	2.4	2562
150	64.5	520	80	2.90	5	180	3.4	3630
165	78.0	629	88	3.51	11.2	207	4.2	4390
180	92.9	749	96	4.18	23.4	264	5.0	5230

Distance = 11.5 Mpc

Total light in B = 22.2 10⁹ L_⊙^B (uncor.)Total gas mass = 18.8 10⁹ M_⊙

Disc scalelength = 4.5 kpc

Bulge scalelength = 397 pc

Disc mass / bulge mass = 18.7

potential, but in general such a disc adaptation is small, certainly if the disc is relatively massive. The dispersions in the radial and tangential directions are related to $\langle v_z^2 \rangle^{1/2}$ as

$$\langle v_z^2 \rangle^{1/2} = 0.6 g(R) \langle v_R^2 \rangle^{1/2}, \quad (12)$$

and

$$\langle v_{\Theta}^2 \rangle^{1/2} = \frac{\kappa}{2\Omega} \langle v_R^2 \rangle^{1/2}. \quad (13)$$

Here $g(R)$ is a function close to 1.0 and will be discussed in the next section. The tangential dispersion $\langle v_{\Theta}^2 \rangle^{1/2}$ is related to the radial dispersion through Ω and κ , which are the orbital and epicyclic frequencies. The average rotation of the stars (v_*) is given as the testparticle rotation, $v_t = \sqrt{(d\Phi/dR)/R}$ diminished with the asymmetric drift:

$$v_t^2 - v_*^2 = \langle v_R^2 \rangle \left[\frac{R}{h} - R \frac{\partial}{\partial R} \ln \langle v_R^2 \rangle + \frac{1}{2} \left(\frac{R}{v_*} \frac{\partial v_*}{\partial R} - 1 \right) \right], \quad (14)$$

using a plane parallel epicyclic approximation. At the radii where the stellar velocity dispersion becomes larger than the rotation, Eq. (14) does not hold any more. For these inner regions an interpolation by hand has been made to $R = 0$. Stellar particles are distributed according to Eq. (10) and are given a rotation according to Eq. (14). Dispersions in the R , z , and Θ directions follow from Eqs (11) to (13) and are drawn from Gaussian distributions.

The gas layer has a radial functionality as observed for NGC 628. The thickness of the gas layer is determined by the surrounding potentials of the other components and the gas velocity dispersion. For the latter a constant, isotropic value of 8 km s⁻¹ has been adopted. To calculate the thickness of the gas layer the (ad hoc) description of Bottema (1996) has been used.

The bulge is spherical with a projected exponential radial distribution, $\sigma_b = \sigma_0^b e^{-r/h_b}$ resulting in a spatial distribution of the bulge density ρ_b of

$$\rho_b = \frac{\sigma_0^b}{\pi h_b} K_0 \left(\frac{R}{h_b} \right). \quad (15)$$

Here h_b is the scalelength of the bulge and K_0 a modified Bessel function. A cutoff to the bulge density is taken at eight bulge scalelengths. For the dark halo the usual pseudo isothermal sphere is assumed with a density ρ_h of

$$\rho_h = \rho_0^h \left[1 + \frac{R^2}{R_{\text{core}}^2} \right]^{-1}, \quad (16)$$

and belonging rotation velocity v_h of

$$v_h = v_{\max}^h \sqrt{1 - \frac{R_{\text{core}}}{R} \arctan \left(\frac{R}{R_{\text{core}}} \right)}, \quad (17)$$

where R_{core} is the core radius of the halo related to the maximum rotation v_{\max}^h by

$$v_{\max}^h = \sqrt{4\pi G \rho_0^h R_{\text{core}}^2}. \quad (18)$$

As template for the model galaxy the beautiful face-on spiral NGC 628 is used. It has a regular spiral structure and certainly not a bar. This gives the possibility to compare the structure resulting from the simulations with an actual galaxy in an unambiguous way. It is not intended to make a model of NGC 628 in all its details, but only to generate a galaxy which has roughly the same dimensions. Photometry of NGC 628 is presented by Shostak & van der Kruit (1984) and by Natali et al. (1992). The first authors give a disc scalelength for the Kodak J emulsion of 85'' while the second authors give $h_d = 73''$ in the R-band. As a compromise I shall use a value of 80'' which gives for an adopted distance of 11.5 Mpc a value of $h_d = 4.5$ kpc. A photometric disc profile with that scalelength has been subtracted from the photometry of Natali et al. and to the remaining central bulge light an exponential has been fitted. From that follows a bulge scalelength of $7''.12 = 397$ pc and the surface brightness of bulge and disc are equal at a radius of $15''.3$. This photometric analysis gives the absolute scales and brightness ratio of bulge and disc but not yet the masses of these components.

NGC 628 is observed in H I by Wevers et al. (1986) who give the radial H I gas density. This profile is supplemented with the H₂ radial profile as observed by Combes & Bica (1997) and the total is multiplied with a factor 1.4 to account for Helium. The resulting radial gas profile as it has actually been used is given in Fig. 2. Note that although the addition of H₂ in the centre looks quite impressive, it only contributes 8.5% to the total gas mass of $18.8 \cdot 10^9 M_{\odot}$.

Because NGC 628 is face-on its rotation curve cannot be measured. Yet for its absolute luminosity and Hubble type the Tully-Fisher relation of Rubin et al. (1985) gives

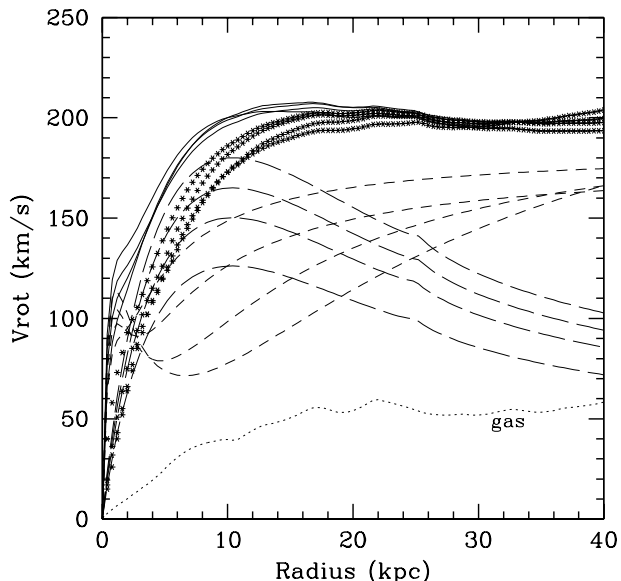


Figure 3. For the photometry and gas content of NGC 628 a decomposition has been made of an adopted rotation curve reaching a flat level of 200 km s^{-1} (full drawn line). Four different disc masses are considered corresponding to maximum disc rotations of 126, 150, 165, and 180 km s^{-1} (long dashed lines). The combined halo plus bulge rotation (short dashed lines) is then adjusted to fit the adopted total rotation. For each disc contribution the stellar rotation is given by the asterisks.

a maximum rotation of approximately 200 km s^{-1} . This value has been adopted as the exact maximum rotation for the model galaxy together with the observational establishment that rotation curves are flat in the outer regions of a galaxy. For the exponential disc rotation curves have been calculated (Casertano 1983) scaled to four different maximum rotational values of 126, 150, 165, and 180 km s^{-1} . These four stellar discs all have a certain mass and mass-to-light ratio. Combined with each disc is a bulge density distribution where equal M/L ratios of bulge and disc have been assumed. For the four cases a dark halo has been created such that the total rotation is approximately flat at 200 km s^{-1} . The result of this fitting procedure is shown in Fig. 3 and numerical values are presented in Table 1. Also given in Fig. 3 is the actual stellar rotation which results after the subtraction of the asymmetric drift, in this case for a z_0 value of 900 pc.

4 PRACTICAL PROPERTIES AND ADAPTATIONS

4.1 Main parameters

To gain insight into the possible morphologies of a disc, the main structural parameter to be investigated is the ratio of maximum disc rotation to total rotation: $v_{\text{disc}}^{\text{max}}/v_{\text{obs}}^{\text{max}}$. Though it has already been known since the calculations by Ostriker & Peebles (1973) that a galaxy where the disc approaches its maximum disc limit is unstable to bar formation, (see also Bottema & Gerritsen 1997) that notion should be confirmed for an actual 3D disc with gas and

star formation. Inevitably related to the matter of stability must be the thickness of the disc. A thicker disc has a larger vertical velocity dispersion. The dispersions in the three directions are related, which means that a thicker disc has a larger Q value and should at least be more stable to local distortions. Therefore z_0 is the second main parameter to be investigated.

The precise amount and the process by which mechanical SN energy is transferred to the gas is not known. Consequently the influence of the parameter ε_{SN} will be considered in some detail. A fourth parameter has been added during the course of the simulations. For a resulting SFR of $4 M_{\odot} \text{ yr}^{-1}$ it appeared that the gas reservoir becomes depleted pretty fast. To create a constant situation over a reasonable time span, gas has been added at several rates. Summarizing, the main parameters investigated in this paper are: $v_{\text{disc}}^{\text{max}}/v_{\text{obs}}^{\text{max}}$, z_0 , ε_{SN} , and gas supply.

4.2 Particle masses and numbers

For most simulations the number of stellar particles was 150.000 and the number of gas particles 16.000, though some simulations are presented using 40.000 gas particles. In Table 1 the total stellar disc masses are given for the various maximum disc rotations. From $v_{\text{disc}}^{\text{max}} = 126 \text{ km s}^{-1}$ to 180 km s^{-1} the stellar particle masses then range from $0.3 \cdot 10^6$ to $0.6 \cdot 10^6 M_{\odot}$. For a total gas mass of $18.8 \cdot 10^9 M_{\odot}$ and 16.000 gas particles, the mass of one gas particle amounts to $1.18 \cdot 10^6 M_{\odot}$. During the star formation process new stellar particles are created with masses of $\frac{1}{2}$, $\frac{1}{4}$, and $\frac{1}{8}$ of the mass of a gas particle, being comparable to the masses of the already existent stellar particles.

4.3 The star formation rate

The SFR as defined here is the total amount of gas mass which is transformed into stellar mass, per time unit. In the code no stellar mass is returned to the gas reservoir. For an actual galaxy with a standard IMF, approximately 70% of the gas that has formed stars is eventually locked up in old stars and stellar remnants. The other 30% is returned, of which most in a short time scale after SF. Because this time scale is so short the non returning of gas in the numerical simulations is a good approximation. However, the star formation rate that could be observed is then not equal to the SFR as defined above. For a lock up rate of 70% the “observable SFR” is defined as $1/0.7$ times the SFR and can as such be compared with observations. Kennicutt (1983) has determined an “observable SFR” of $3.8 M_{\odot} \text{ yr}^{-1}$ for NGC 628, when it is put at a distance of 11.5 Mpc. There is a systematic error of approximately a factor of two associated with this value of $3.8 M_{\odot} \text{ yr}^{-1}$ mainly caused by the uncertainty of the IMF.

4.4 Stochastic heating

An average galactic disc is essentially collisionless. In a simulation a disc is made up of far less particles than the number of stars in a real galaxy. As a result encounters between particles will occur in simulations and the particle ensemble will be heated up. This process of particle scattering is

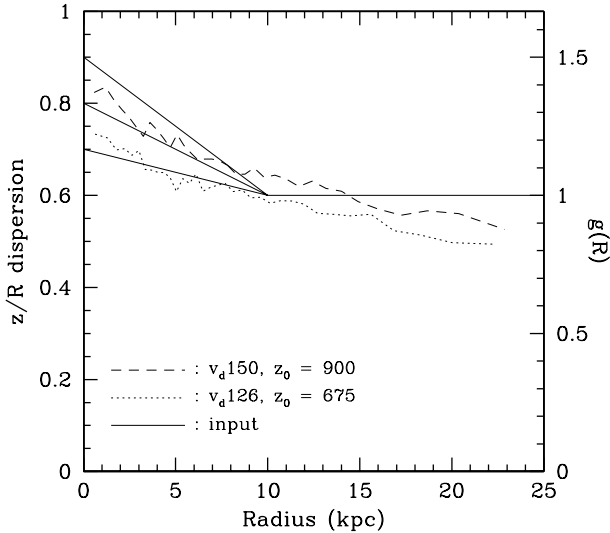


Figure 4. The ratio of vertical to radial stellar velocity dispersion of the model galaxy. The dynamical equilibrium is indicated for two cases: $v_{\text{disc}}^{\text{max}} = 150 \text{ km s}^{-1}$ with $z_0 = 900 \text{ pc}$ and $v_{\text{disc}}^{\text{max}} = 126 \text{ km s}^{-1}$ with $z_0 = 675 \text{ pc}$. Simulations are started with the functionality given by the “input” line with a z/R dispersion at $R = 0$ of 0.9, 0.8, 0.8, and 0.7 for $v_{\text{disc}}^{\text{max}} = 180, 165, 150$, and 126 km s^{-1} respectively.

commonly referred to as stochastic heating. In practice this means that a model disc made up of a limited number of particles will heat up, get thicker, and become more stable during a simulation.

In a real galaxy which contains gas, stellar heating may be generated by two processes. At first heating by encounters of stars with molecular clouds (Spitzer & Schwarzschild 1953; Villumsen 1985). Secondly a more effective mechanism seems to be heating by transient spiral structures (Barbanis & Woltjer 1967; Carlberg & Sellwood 1985) though in practice a combination of both mechanisms is likely taking place. In a simulation with a limited number of stars, and with spiral arms and cloud complexes both, stochastic heating and real heating will take place. The problem is to disentangle the two.

This disentanglement can be done by considering the change of the stellar velocity dispersion. From basic principles one can derive for stochastic heating that

$$\frac{d\langle v^2 \rangle}{dt} \propto \frac{\ln N}{N}, \quad (19)$$

such that the change of the square of the velocity dispersion is proportional to a function of the number of particles N . During a simulation the square of the velocity dispersion will increase by stochastic heating and by heating of clouds and arms. If the same simulation is repeated for different numbers of stellar particles both heating processes can be disentangled. Another way to study the matter is by comparing the same simulations with and without gas, as long as the gasless simulation produces a smooth featureless disc. Using these methods, a small investigation was done for a simulation using $v_{\text{disc}}^{\text{max}} = 150 \text{ km s}^{-1}$ and $z_0 = 675 \text{ pc}$. It appears that for a total of 180.000 stellar particles the disc does not show stochastic heating at a radius of one scale-

length and shows it barely at two scalelengths. As a final compromise a number of 150.000 stellar particles has been used for all discs. This means that beyond a radius of approximately two scalelengths a small amount of heating will be present, not occurring in real galaxies.

4.5 The softening length

When performing 2D simulations of discs, the thickness is generally artificially implemented by taking a stellar softening of size comparable to the scaleheight of the disc. The particles then do not meet in the plane but a disadvantage of this adaptation is a considerable additional stabilization compared to a 3D situation with the same dimension and kinematics (Romeo 1994).

For 3D simulations considerations on the size of the softening length have been made by Hernquist (1987). It appears that in order to achieve a good approximation of the force computation the softening length should be smaller than λ , being the mean interparticle distance at the half mass radius. For an exponential disc Hernquist gives an approximation of $\lambda \approx 2.63(N/h^2 z_0)^{-1/3}$ which for the present case of NGC 628 with $N = 150.000$ gives $\lambda \approx 120 \text{ pc}$. One may consider other evaluations of λ , for instance the mean interparticle distance at the half mass height above the plane. In that case λ ranges from $\sim 110 \text{ pc}$ at the centre to $\sim 230 \text{ pc}$ at $R = 2h$. When a bar develops, however, λ may become even smaller in the bar region. Therefore, for the galaxy under investigation in this study the softening length should be smaller than approximately 100 pc.

To get a lower limit on the softening length is more problematic. If ε is too small, strong interactions between particles will occur. That is especially problematic when particles with different mass are present; the lightest particle will then be ejected, carrying with it large amounts of energy and angular momentum. In addition, for close particle interactions the time step may be too small to achieve a correct orbit integration. To investigate matters, pure stellar simulations have been performed for a case where a moderate bar develops (Fig. 10, bottom left) with ε ranging from 2 to 200 pc. For ε between 10 and 200 pc the resulting structure and stellar kinematics is practically equal. For $\varepsilon \lesssim 10 \text{ pc}$ particles get ejected from the galaxy (particles have masses differing \sim a factor two) which changes the eventual morphology. It is therefore concluded that for the present calculations there is a safe range between 10 to 100 pc for the stellar softening length. It has been fixed at 20 pc for all simulations. In no case there will then be artificial stabilization by a too large softening length.

4.6 The quotient of vertical to radial stellar velocity dispersions

In first instance this quotient was put at 0.6 for all radii as an extrapolation of the number for old disc stars in the solar neighbourhood. Consequently the function $g(R)$ in Eq. (12) $\equiv 1.0$ for all radii. During the initial stages of the simulation, for the more massive discs, there appeared to be some outflow of stars from the central regions. A solution to this problem was found after comparing the final quotient for some realistic simulations with the original input (see Fig.

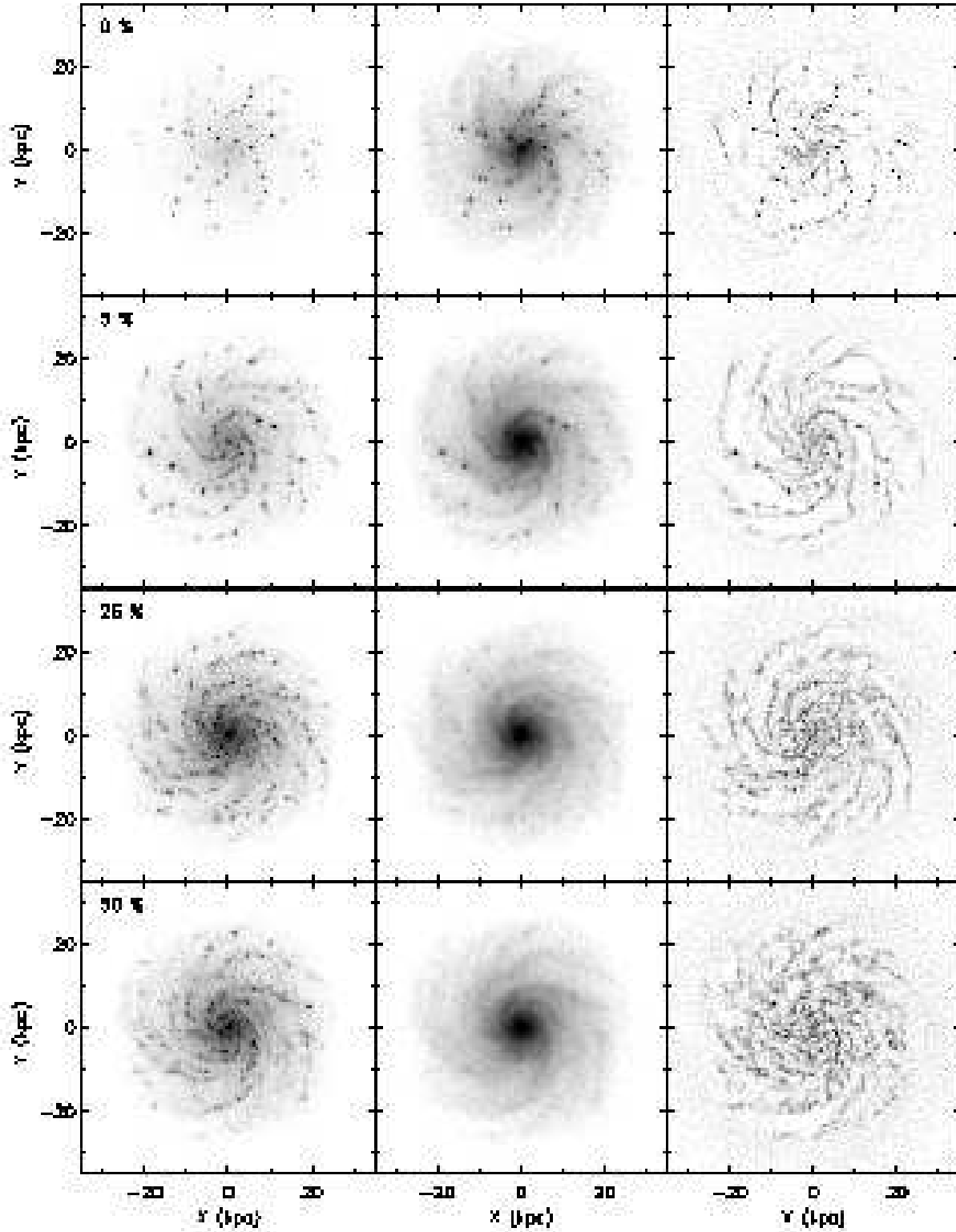


Figure 5. The resulting galaxy after 1.5 Gyrs of simulation. In this and following similar figures the left column gives the simulated V-band image, the middle column gives the stellar mass image and the right column the gas mass. The disc has a maximum rotation of 126 km s^{-1} and z_0 of 675 pc while gas was supplied at a rate of $4 M_{\odot} \text{ yr}^{-1}$. From top to bottom row the mechanical SN feedback efficiency was at 0%, 5%, 25%, and 50%. In case of none or low SN feedback unstable giant SF regions appear. More SN feedback results in a galaxy which is in SF equilibrium having an appearance not unlike that of a real galaxy. High SN feedback destroys the coherent gas spiral structure.

4). At the end of the simulations the velocity dispersion ellipsoid is always more spherical in the inner regions, while it remains at ~ 0.6 near two scalelengths. The initial model galaxy has been adapted to have a function $g(R)$ slightly variable as a function of radius. As shown in Fig. 4, the central quotient was put at 0.7 (for $v_{\text{disc}}^{\text{max}} = 126 \text{ km s}^{-1}$), at 0.8 (for $v_{\text{disc}}^{\text{max}} = 150$ and 165 km s^{-1}) or 0.9 (for $v_{\text{disc}}^{\text{max}} = 180 \text{ km s}^{-1}$) and decreased linearly to 0.6 at a radius of 10 kpc. For such a setup the initial central instability has completely disappeared. For a disc with maximum disc rotation of 126 km s^{-1} or lower this adaptation was, in principle, not necessary; the galaxy slowly changes to the final quotient without noticeable redistribution of matter.

5 CREATING A GALACTIC DISC IN EQUILIBRIUM

5.1 The amount of SN action

The first parameter of which the effect has been investigated is the SN efficiency. To that aim a realization of the model galaxy has been chosen which is close to what observations of galactic discs suggest. Therefore a thickness z_0 of 675 pc is assumed (van der Kruit & Searle 1982) and a disc maximum rotational contribution of 63% (Bottema 1993). By no means the statement is given that this galactic constitution is the closest to reality; only that it is a reasonable assumption and suitable to test the effect of the amount of SN feedback. During the simulations gas has been supplied at a rate of $4 M_{\odot} \text{ yr}^{-1}$ being approximately equal to the amount of gas depletion by SF.

Results of $\varepsilon_{\text{SN}} = 0\%$, 5% , 25% , and 50% are given in Fig. 5 where for each case the simulated V-band image, stellar mass image, and gas mass image is presented. In fact, Fig. 5 is pretty self explainable. If the SN feedback is absent or small, dense clumps of gas and young stars are created, which dominate the V-band and gas image. On these clumps cold gas continues to accumulate and because the density is so large, the cooling outruns the heating by the FUV field of young stars. It should be kept in mind that cooling proceeds proportional to the square of the gas density (Eq. 4) and heating proportional to the first power of the density (Eq. 6) and a runaway process as observed might indeed be expected to occur. For an ε_{SN} of 25% the clumping process has almost completely disappeared and a number of spiral arms appear in the stellar light, mass, and gas distribution. Certainly in the gas structure these arms have a certain width contrary to the lower ε_{SN} simulations where the gas arms are thin and have a threaded appearance. Increasing the supernova feedback to the high value of 50% results in the creation of multiple holes in the gas structure. The feedback is now so violent that spiral arms in the gas image have all but disappeared. As a result also the strength of the spiral arms in the light and stellar mass images decreases.

For the different SN feedback situations the resulting SFR as a function of time is presented in Fig. 6. In case of low ε_{SN} and the generated severe clumping the SFR keeps on increasing, evidencing the runaway star formation process. If this would continue, the galaxy gets quickly depleted of its gas and the SF activity would subside again. A larger SN feedback results in a lower SFR, though above $\varepsilon_{\text{SN}} =$

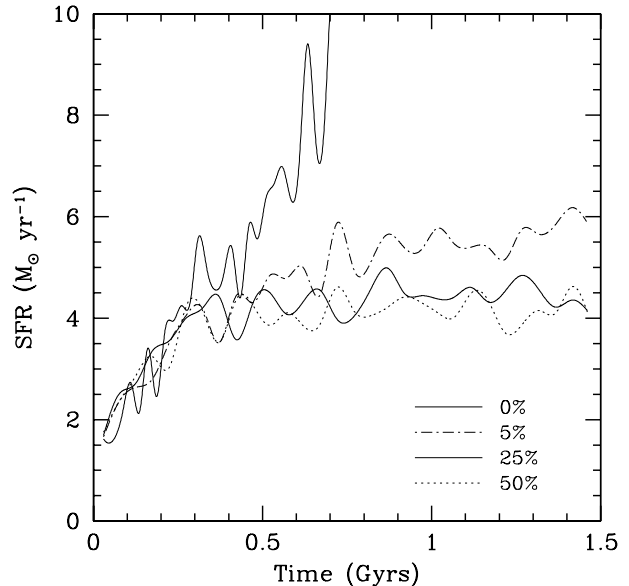


Figure 6. The star formation rate during the simulations presented in Fig. 5. For low efficiencies of the SN feedback (0 and 5%) SF is boosted in numerous giant SF regions. A larger SN feedback results in an equilibrium situation at which the SFR reaches a constant level determined by the gas supply and cooling function.

25% the SFR remains more or less constant at a level of $4.2 M_{\odot} \text{ yr}^{-1}$. Corrected for stellar mass loss (Sect. 4.3) this gives $6 M_{\odot} \text{ yr}^{-1}$ which is in good agreement with the observed value for NGC 628 (Kennicutt 1983). There is no evidence for the process of stochastic self propagating SF by supernovae explosions (Mueller & Arnett 1976; Elmegreen 1992). On the contrary, more SN action decreases the amount of SF when the SN action is low, while for higher regimes of SN action the SFR seems to be almost independent of the amount of SN feedback. During the simulations star formation occurs mainly by cooling and dissipation of the gas. SN action prevents a runaway SF process and influences the gas morphology.

An investigation has been made of how the structures and relations of Fig. 5 depend on other parameters. It does not depend on the value of M_{crit} (Eq. 7). There is a dependence, however, on the value of the collapse factor f_c (Eq. 8). If the time span before star formation is increased from the nominal value of $0.5 \times t_{\text{ff}}$ the relative amount of cold ($T < 500 \text{ K}$) gas increases and the clumping process sets in at higher SN feedback values, and vice versa. Since the ratio of cold to warm H I gas is as yet undetermined it is impossible to pinpoint down the exact value of ε_{SN} (see Sect. 7 for an ample discussion). Still, following indications of the observations leading to the adopted values for the parameters, the relation between the morphology in Fig. 5 and the value of ε_{SN} is likely accurate to within a factor of two.

5.2 Different amounts of gas supply

As noted before, it became evident during this investigation that when having a gas consumption rate of $\sim 4 M_{\odot} \text{ yr}^{-1}$ for a total gas amount of $18.8 \cdot 10^9 M_{\odot}$, the gas gets depleted

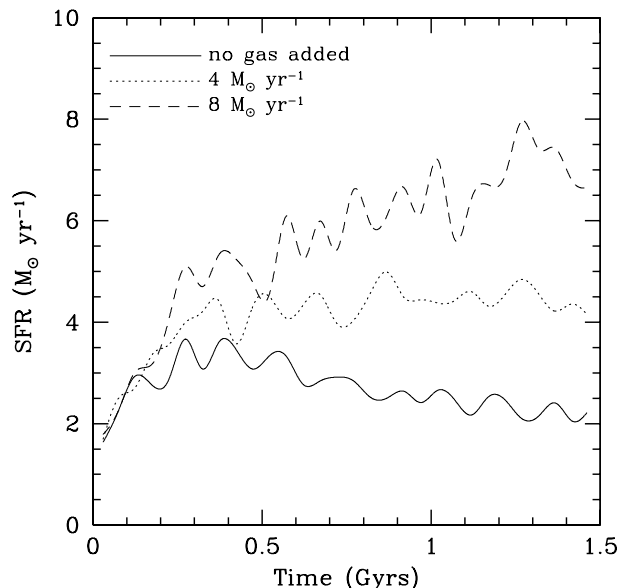


Figure 7. The star formation rate during simulations with different amounts of gas supply. Eventually the SFR will adjust itself to the amount of gas that is being added.

pretty fast. In the mean time, it takes a while, let's say some $0.8 \cdot 10^9$ yrs, before a stable galaxy emerges (see Fig. 6). To have a constant gas reservoir over at least this adjustment time it was decided to create the possibility to add gas at a certain rate. For a real galaxy it is also expected that gas gets accreted, although the way how is (still) unclear. Therefore this gas suppletion is less artificial than it might seem.

Care has been taken that the addition of gas does not alter the available gas structure. For example, gas should not be supplied at those positions where it has just recently been removed by star formation. Gas particles have been added randomly by selecting another gas particle and placing the new gas close to that selected particle. From this selection are excluded gas particles with temperatures above 20,000 K or below 5000 K. Also excluded are, of course, SN particles or particles already Jeans unstable. It became clear that when gas is added at places beyond the stellar disc, that only increases the amount of gas over there, taking more computing time, and not replenishing the gas where it is depleted. Therefore no gas has been added at radii larger than 25 kpc. It was originally expected that extra gas at large radii would slowly migrate inwards by dissipation and viscous interaction. That process, however, did not take place.

The morphology and SFR of a galactic disc has been investigated in cases of gas addition of 0, 4, and $8 M_{\odot} \text{yr}^{-1}$ during a period of $1.5 \cdot 10^9$ years. A disc is chosen equal to the one where the amount of SN action was investigated, with a fixed ε_{SN} of 25%. A SFR at a constant level is achieved when $\sim 4 M_{\odot} \text{yr}^{-1}$ is added. When no gas is added the SFR approaches $4 M_{\odot} \text{yr}^{-1}$ after 3 to $4 \cdot 10^8$ years from the start of the simulation, and declines gradually thereafter (see Fig. 7). At the end of the simulation the SFR has decreased to $2 M_{\odot} \text{yr}^{-1}$. As can be seen in Fig. 7, when gas is added at $8 M_{\odot} \text{yr}^{-1}$ the SFR keeps on increasing to reach eventually the level of gas input. In this way one can draw an impor-

tant though not unexpected conclusion: the SFR in a disc adjusts itself to the amount of gas that is being supplied. The time scale on which this happens is for the present simulation ~ 1 Gyr, but will likely depend on the numerical resolution. When the images of the galaxy are inspected at 1.5 Gyrs after the start of the simulation it appears that the morphology is only slightly dependent on the amount of gas supply and consequently also only slightly dependent on the actual SFR. More gas and higher SFR results in a somewhat stronger and less regular spiral pattern. When $8 M_{\odot} \text{yr}^{-1}$ is added also a few dense gas clouds develop.

5.3 Comparison with observations

The V-band images as presented in the left column of Fig. 5 are made to resemble a galaxy as depicted in an optical photograph. To that aim the intensity is given on a square-root gray scale and cut off (saturated) above a certain level. There is always some subjectiveness involved in selecting the scale and cutoff and for the best result I aimed at achieving the best overall contrast. In reality, however, this will be equal to the process of developing and printing of actual photographs. A shortcoming of the simulations is the lack of dust. Certainly the young SF regions in real galaxies are often (at least partly) enshrouded in some amount of dust, a situation that cannot be reproduced. Another problem is that every new star particle (= SF region) has an IMF going up to stars of $125 M_{\odot}$ which will completely dominate the light in every passband. In a real galaxy there are only a few SF regions which contain such massive stars. To compensate, at least in part, for the lack of dust and for the discrete appearance of very massive stars, the V-band image is made for all the stars at an age $3 \cdot 10^7$ years older than the actual age of the stars. The net effect of this procedure is an image less dominated by young star clusters. Admittedly, there is some artificiality in creating a simulated V-band image to compare with photographs, but there is no way around this.

When there is no SN action the V-band image is completely dominated by bright H II regions and to my knowledge such a galaxy does not exist. For $\varepsilon_{\text{SN}} = 5\%$ the optical image is also very knotty and is barely consistent with the image of NGC 628 on, for example, page 99 of the Shapley-Ames catalog. When ε_{SN} is larger the optical images are not unlike images of real galaxies. The problem with the stellar mass images is that these cannot be observed. Even in the near infrared passbands young populations will supply extra light, e.g. have a smaller M/L ratio compared to an old population.

Contrary to the optical and stellar mass image, the image of the gas can actually be compared with observed H I structures. High resolution H I observations of nearby late type galaxies are presented by a.o. Braun (1995) and Kamphuis (1993). Such a high resolution is necessary because one would like to compare the small scale gas structure and in particular the size and distribution of holes created by SN feedback. For example, Fig. 5 lower right panel shows lots of small holes and cavities in the inner region, all created by SN explosions. In addition, a particular feature of SN feedback are holes blown into the ridge of spiral arms. This can be witnessed in the same image at for example positions (x,y) = (5,-15) and (-4,19). The observations of the gas structure do never show the knotty and threaded gas structures as for

$\varepsilon_{\text{SN}} = 0$ and 5%. The best resemblance between simulations and observations is for ε_{SN} around 25%, though also more amorphous gas structures resembling the structure for $\varepsilon_{\text{SN}} = 50\%$ are observed. A complicating factor is that some of the nicest H I spiral structures are observed in galaxies with grand design spiral arms obviously caused by an interaction with other galaxies, for example M81 (= NGC 3037). In such cases gas becomes aligned with the gravitational spiral disturbance, influencing its global appearance. This should be taken into account when comparing the simulated gas structures with real observations.

5.4 Whence spiral arms?

The spiral structure which is generated in the present simulations of an isolated galaxy is the result of an equilibrium of four actions. On the one side cooling and dissipation accumulates the gas in threads and clumps. This is counteracted by FUV heating and SN feedback. If the latter action is too small the gas collapses completely into a few giant SF regions. On the other hand, if the action of heating and SNs is too large, warm gas get dispersed over the disc preventing the formation of any coherent structure. Except for this amount of mechanical feedback the resulting gas and mass structures do not depend on details (like IMF, M_{crit} , etc) of the star formation process (see Sect. 5.1 and G197). It is therefore likely that these structures do not depend on the exact star formation recipe.

The behaviour of the gas is the main cause of structure formation. As a result the underlying stellar mass distribution becomes disturbed and also in the stellar disc spiral arms are formed. In this way gas mass enhancements more or less swing amplify the stellar mass into a spiral structure. But this is probably not the whole story. If it were only the need of mass accumulations to generate spirals, then it is expected that the low ε_{SN} situation with its specific clumps would generate the strongest spirals. Obviously that is not the case. The gas enhancements really have to be wound up in spirals by the differential rotation to create an accompanying mass enhancement. A situation is established where shearing gas filaments swing amplify the underlying mass distribution into a transient small scale density wave. The latter appears as a spiral arm. More insight is gained when the simulation is played as a movie on the TV screen. It can then be noticed that coherent spiral features develop and exist for approximately half a rotation period. Spiral arms are “wound” into existence and disappear by winding and stretching too much or by interaction with other spiral features. Such interactions also create the typical bifurcation patterns of the arms often seen in real galaxies. Not created in the present simulations are the grand design $m=2$ spirals witnessed in a few exemplary galaxies. These matters will be further investigated and discussed in sections 8 and 9.

6 THE BAR INSTABILITY

6.1 The appearance as a function of disc mass

An amount of SN feedback has now been determined which results in a good resemblance with observed structures in

a disc while for a gas addition of $4 M_{\odot} \text{yr}^{-1}$ the gas reservoir remains constant. Fixing these parameters and fixing the thickness parameter z_0 at 900 pc the resulting morphology for different disc contributions to the total rotation has been investigated. Images of the galaxy after $1.5 \cdot 10^9$ years of simulation are presented in Fig. 8 for $v_{\text{disc}}^{\text{max}}$ of 126, 150, 165, and 180 km s^{-1} . As for Fig. 5, Fig. 8 speaks pretty much for itself. Discs with a moderate rotational contribution of 126 and 150 km s^{-1} evolve into a regular spiral galaxy. For $v_{\text{disc}}^{\text{max}} = 150 \text{ km s}^{-1}$ there appear to be less arms which are more pronounced than in the case of $v_{\text{disc}}^{\text{max}} = 126 \text{ km s}^{-1}$. However, the images presented in Fig. 8 are only one snapshot at one particular time. During the simulations arms come and go and are variable in strength. Judging the whole simulation from $t = 0$ to $t = 1.5 \cdot 10^9$ years the $v_{\text{disc}}^{\text{max}} = 150 \text{ km s}^{-1}$ case has also on average a slightly more pronounced spiral structure.

Discs with a larger rotational contribution obviously develop a bar. For $v_{\text{disc}}^{\text{max}} = 165 \text{ km s}^{-1}$ the disc starts out by forming a few large and broad spiral structures, a situation which continues to $\sim 1.2 \cdot 10^9$ year. Then quite suddenly the bar appears. For $v_{\text{disc}}^{\text{max}} = 180 \text{ km s}^{-1}$ the simulation also sets out by forming broad dominant spiral features which already after $\sim 0.5 \cdot 10^9$ years settle into a barred structure. When the bar is present gas is transported inwards rapidly along the bar. The same conclusion was reached by Athanassoulas (1992) for simulations of gas moving in a rigid barred potential. That study shows that the gas is transported inwards along shocks appearing on the leading side of the bar. The present calculations give the same results, though the resolution is not good enough to investigate details of this process.

In the bar the gas density is large, cooling is fast and new stellar particles form in appreciable quantities. So much young stars form at some positions and certainly at the centre that FUV heating outweighs the cooling and gas remains at $\sim 10^4 \text{ K}$ while becoming ever more dense. When gas particles accumulate within the softening length numerical problems occur. To avoid these, the gas was forced to form new stars above a density limit of $10 M_{\odot} \text{pc}^{-3}$ even though the star formation criteria of subsection 2.4 were not yet satisfied. It was not intended and it is not possible to simulate the processes going on at the very centre of the bar region. What the simulations do show is that gas is transported inwards along the bar, where it forms stars at a considerable rate. As a consequence a concentration of young stars emerges at the inner few kpc which takes on a more or less spherical shape. This can be called the development of a bulge. For the whole galaxy the radial luminosity profile changes from exponential to Freeman type II (Freeman 1970) where the shoulders of the profile coincide with the bar. Getting back to Fig. 8, one can notice the effect of the inwards gas transport. For $v_{\text{disc}}^{\text{max}} = 180 \text{ km s}^{-1}$ the bar has existed longer than for $v_{\text{disc}}^{\text{max}} = 165 \text{ km s}^{-1}$. As a consequence in case of $v_{\text{disc}}^{\text{max}} = 180 \text{ km s}^{-1}$ the region around the bar has already been severely depleted of gas. The results of the present simulations of the barred galaxies are identical to those of Friedli & Benz (1995). They also specifically report the gas inflow, SF along the bar and in the centre, and the formation of a bulge.

But, do we need the gas to form or not to form bars? To investigate this, the simulations presented in Fig. 8 have

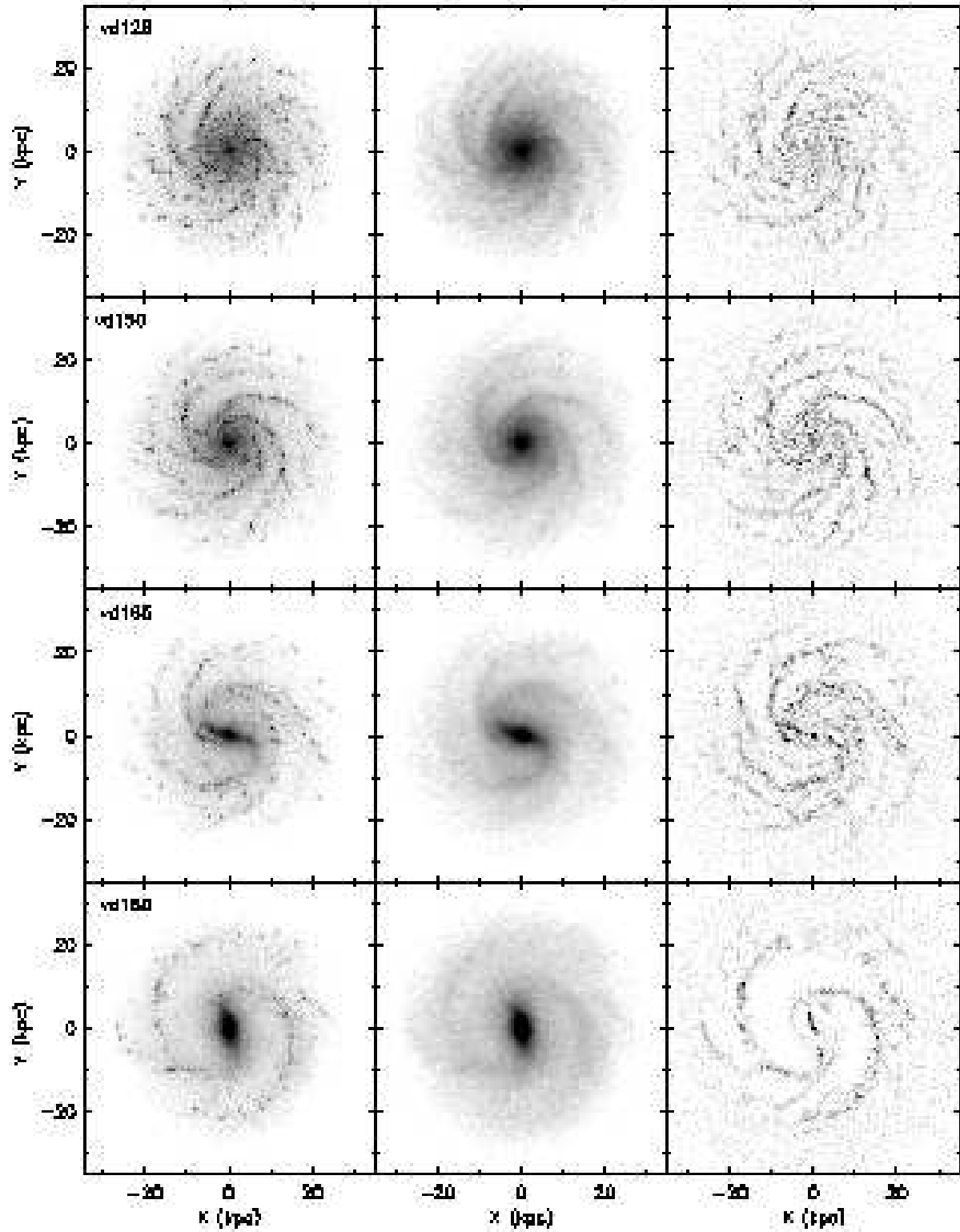


Figure 8. For a fixed SN efficiency of 25%, gas suppletion rate of $4 M_{\odot} \text{yr}^{-1}$, and $z_0 = 900$ pc, the resulting galaxy after 1.5 Gyrs of simulation is presented for four values of the maximum rotation of the disc (126, 150, 165, and 180 km s^{-1}). Less massive discs evolve into a regular spiral galaxy, while more massive discs develop a bar. In case of a bar, gas is transported inwards as can be noticed in the right column.

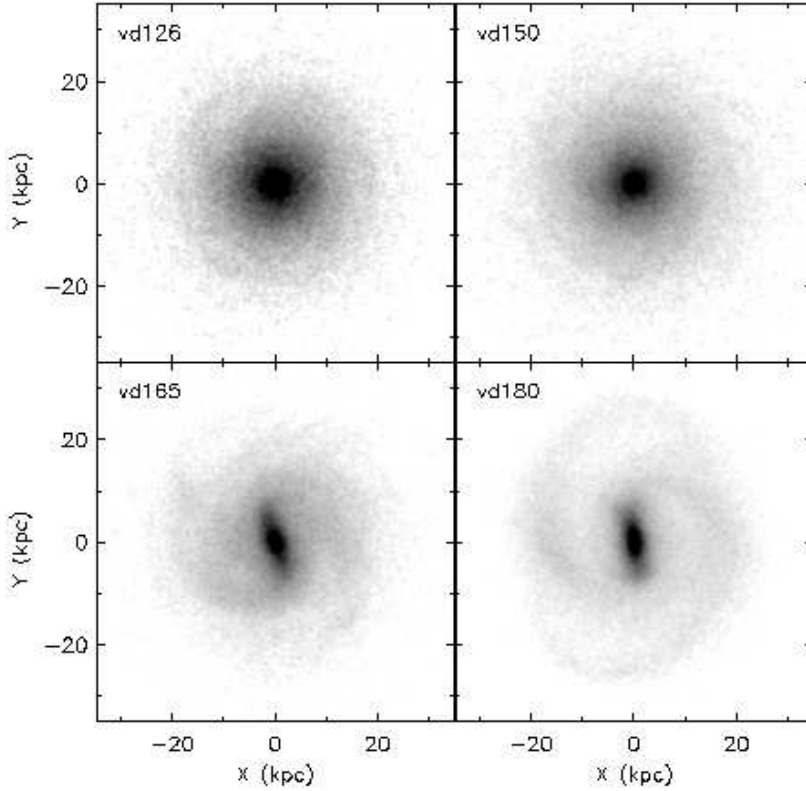


Figure 9. The stellar mass image of the same four galaxies presented in Fig. 8 after 1.5 Gyrs of simulation, but now the gas is replaced by stars. Without gas the bar does, or does not, appear just as well. It is obvious, though, that gas is needed to generate spiral structure.

been re-run without gas. In order to obtain nearly the same density structure and same rotation curves the gas has been replaced by stellar particles which were given the same sech^2 vertical distribution as the other stars. The resulting density structure after $1.5 \cdot 10^9$ years is given in Fig. 9. For $v_{\text{disc}}^{\text{max}} = 165$ and 180 km s^{-1} the structure closely resembles the mass structure in case gas is included. Only the central regions are less pronounced because no (gas) mass has been transported inwards. Anyway, the conclusion is straightforward; gas is not essential for the formation of bars, at least for the galactic constitution investigated presently. Yet, when inspecting Fig. 9 for the cases of $v_{\text{disc}}^{\text{max}} = 126$ and 150 km s^{-1} another fact is obvious. Namely that gas is essential for the formation of spiral arms. If there is no gas the galactic disc is featureless, while if gas is included, the top two rows of Fig. 8 show that a rich spiral structure may develop.

6.2 Q

Although in principle not applicable for global instabilities, Toomre's (1964) Q criterion is often invoked to assess the dynamical state of a galactic disc. When rigorously applied, Q can then serve as a kind of galactic thermometer, but this rigorous application has its problems as we shall see. Toomre's Q value indicates when an infinitely thin pure stellar disc becomes unstable to local instabilities. It is defined as

$$Q = \frac{\langle v_R^2 \rangle^{1/2} \kappa}{3.36 G \sigma}, \quad (20)$$

where σ is the stellar surface density and κ the epicyclic frequency given by

$$\kappa^2 = \frac{2v_c}{R} \frac{\partial v_c}{\partial R} + \frac{2v_c^2}{R^2}, \quad (21)$$

where v_c is the circular test particle rotation. Q is thus defined there where the epicyclic approximation holds, meaning $\langle v_R^2 \rangle^{1/2} < v_c$. This leads to the first reason why the Q criterion does not apply for bars. Bars develop in the central regions of galaxies which have a large disc mass contribution. At exactly these regions and for those circumstances the epicyclic approximation clearly does not hold. The second reason is, of course, that it is a local and not a global criterion.

To give the Q thermometer for the four simulations of Fig. 8 it has been calculated as a function of radius. This calculation involves a third problem; what to use for v_c and for σ in case of a disc with both stars and gas? If dispersions are small the stellar rotation (v_*) is nearly equal to the test-particle (\sim gas) rotation and it does not matter whether one inserts v_* or v_{gas} for v_c . But in the inner regions of massive discs the asymmetric drift is large and it does matter for the value of Q which rotation is used. Inclusion of a gas component will decrease the effective Q value as demonstrated for a thin disc by Bertin & Romeo (1988). For a real galaxy a straightforward recipe for the conversion of Q so as to include the gas cannot be given. To make a first attempt one might substitute $\sigma_* + \sigma_{\text{gas}}$ for the surface density σ in Eq. (20). In this way I was lead to define two Q values, a pure stellar one (Q_*) defined as

$$Q_* = \frac{\langle v_R^2 \rangle^{1/2} \kappa_*}{3.36 G \sigma_*}, \quad (22)$$

and a Q_t given by

$$Q_t = \frac{\langle v_R^2 \rangle^{1/2} \kappa_{\text{gas}}}{3.36 G(\sigma_* + \sigma_{\text{gas}})}, \quad (23)$$

the two of which should give an unambiguous description of the value and range of the Q thermometer. The result is given in Fig. 10. The replacement of v_* by v_{gas} has an effect on Q only at the inner regions. On the other hand, for large radii and especially for the least massive discs the inclusion of the gas surface density leads to a substantial decrease of Q . Only the two most massive discs form a bar. Reading the Q thermometer in Fig. 10 it can be noticed that for these galaxies both Q_* and Q_t fall below 1.2 at certain inner radii. It is also at these positions where the bar eventually develops. Further simulations with different galaxy constitutions (next subsection) show that a level of $1.2 \pm \sim 0.1$ for any minimum Q is indeed critical for bar (in)stability.

There is a small complication, however. As noted in subsection 4.6, an initially constant vertical to radial velocity dispersion ratio of 0.6 changes into a different functionality expressed in the function $g(R)$ of Eq. (12) and displayed in Fig. 4. For discs with $v_{\text{disc}}^{\text{max}} \geq 150 \text{ km s}^{-1}$ the setup has been adapted to accommodate this changing dispersion ratio. For $v_{\text{disc}}^{\text{max}} = 126 \text{ km s}^{-1}$ this was not necessary because that situation settles gently, without mass transport into a stable state with a specific $g(R)$. But a different dispersion ratio results in a different Q value. If the disc mass is fixed, Q can be expressed as

$$Q \propto \frac{\sqrt{z_0}}{g(R)}, \quad (24)$$

which means that if $g(R)$ is larger than 1.0 as it is in the inner regions, Q is smaller than when the dispersion ratio were 0.6 everywhere. As a consequence, for $v_{\text{disc}}^{\text{max}} = 126 \text{ km s}^{-1}$ Q evolves to slightly lower values as demonstrated in Fig. 10 by also showing $Q(R)$ after 1.5 Gyrs. For $v_{\text{disc}}^{\text{max}} = 150 \text{ km s}^{-1}$ the radial functionality of Q_* after 1.5 Gyrs is indistinguishable from the $t = 0$ situation demonstrating that the input $g(R)$ was close to its eventual value. Equation (24) shows another important relation. To increase Q by making the disc thicker is not easy. For example, to bring up Q from 1.0 to a stable $Q = 2$, the value of z_0 has to be increased by a factor four. This changes $h/z_0 = 5$ into $h/z_0 = 1.25$ and the disc is in principle not a disc any more.

6.3 A bar stability criterion

The matter of bar (in)stability has been further investigated by performing a number of simulations for discs with various masses and thicknesses. As noted above, the stability depends on the precise value of $g(R)$ and as a consequence an initial situation should be close to having its equilibrium vertical to radial dispersion ratio. For the four different disc masses with belonging maximum rotation a good approximation to this equilibrium was found by the functionality given in Fig. 4. In each case the thickness parameter z_0 was changed until stability changed into instability or vice versa.

The results of this investigation are summarized in Table 2 and graphically in the $(v_{\text{disc}}^{\text{max}}, z_0)$ plane in Fig. 11. Even for $v_{\text{disc}}^{\text{max}} = 126 \text{ km s}^{-1}$ a bar can be generated when the disc is made thin and cool enough. On the other hand, for the

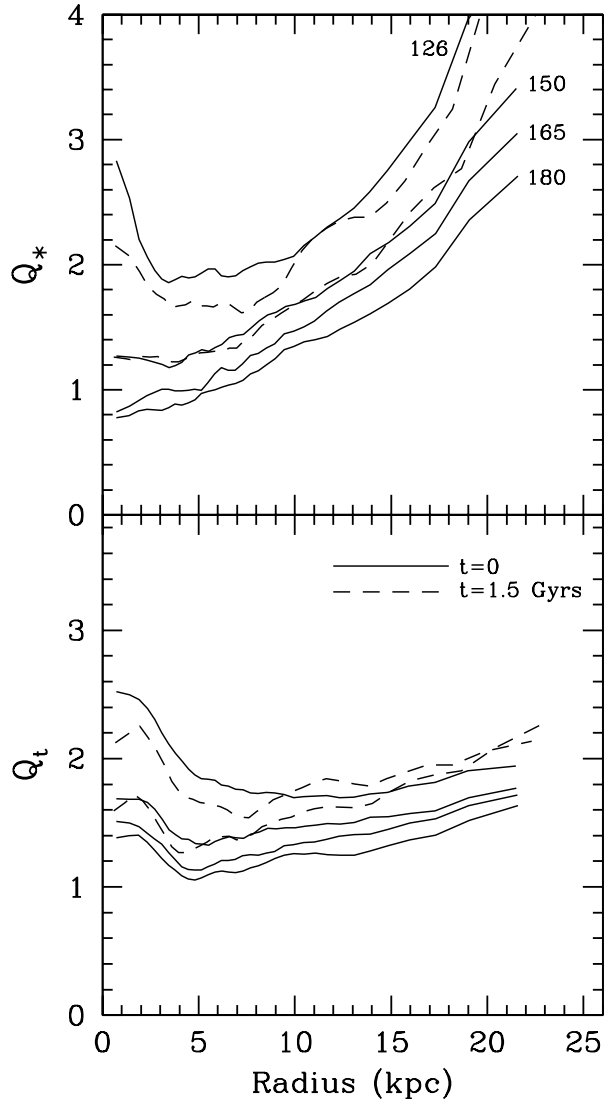
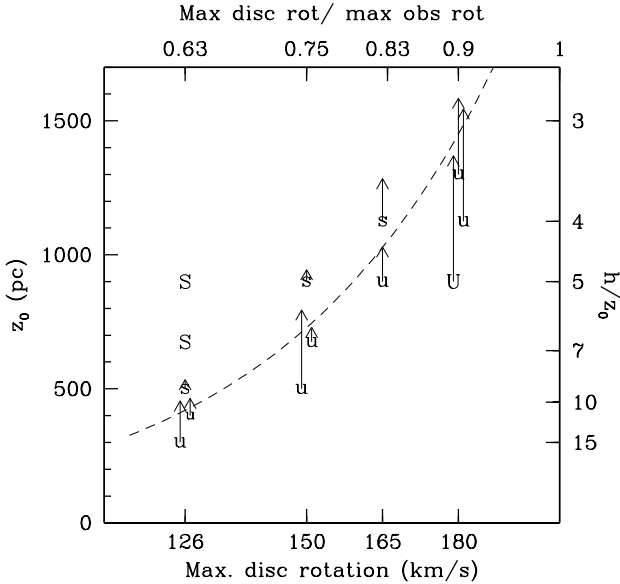


Figure 10. The initial ($t = 0$) value of the Q parameters (Q_* : Eq. 22 and Q_t : Eq. 23) for the four galaxies of Fig. 8 ($z_0 = 900 \text{ pc}$, $\varepsilon_{\text{SN}} = 25\%$). For the stable discs Q is also given at $t = 1.5$ Gyrs by the dashed lines. When any Q falls below ~ 1.2 at certain radii a bar develops.

maximum disc case of $v_{\text{disc}}^{\text{max}} = 180 \text{ km s}^{-1}$ it seems impossible to avoid a bar. For a very thick disc with $z_0 = 1300 \text{ pc}$ a bar still appears. To make the disc even thicker, one needs large stellar velocity dispersions and the epicyclic approximation cannot be applied over most of the radial extent. A determination of the proper asymmetric drift then becomes problematic. For the more massive discs a long bar develops, while the size of the bar decreases towards the less massive discs. The dependence of this bar length on the thickness of the disc seems to be small. In this way one might determine the disc contribution to the total rotation for a barred galaxy by relating the length of the bar to the scalelength of the disc. Unfortunately, the radial photometric profile of barred galaxies is often of an extreme Freeman type II (Freeman 1970) making it difficult to assign a scalelength. The simulations of barred galaxies also show such an evolution

Table 2. Bar stability investigation

Disc v_{\max} (km s ⁻¹)	z_0 $t = 0$ (pc)	z_0 $t = 1.5$ Gyrs (pc)	Bar length (kpc)	Time of bar appearance (Gyrs)
126	300	450	5	0.6
126	400	460	3.5	0.75
126	500	530	stable	
126	675	675	stable	
126	900	900	stable	
150	500	790	8.5	0.75
150	675	725	7	0.6
150	900	940	stable	
165	900	1025	13	1.2
165	1125	1280	stable	
180	900	1365	15	0.45
180	1125	1540	16	0.75
180	1300	1580	16	1.2

**Figure 11.** Results of the bar stability investigation for discs with various masses and thicknesses. A “U” means that a bar develops, in case of an “S” a bar does not develop. The arrows indicate the heating and following thickening of the stellar disc after 1.5 Gyrs. A division of the $(v_{\text{disc}}^{\max}, z_0)$ plane in a stable and unstable section can be made according to Eq. (25) which is represented by the dashed line.

towards type II and suggest that the original scalelength can best be retrieved by taking a global average of the eventual profile in the logarithmic domain.

In Fig. 11 a number of sampling points are given alongside the instability threshold. Of course, more intermediate cases could have been simulated but the results now gathered already give a good impression. When the unstable (U) and stable (S) data points of Fig. 11 are plotted in a $\log(z_0/h)$ versus $v_{\text{disc}}^{\max}/v_{\text{obs}}^{\max}$ plane, a division by a straight line into a stable and unstable section can be made. This dimensionless division line is parameterized by

$$\frac{z_0}{h} = 5.17 \cdot 10^{-3} \exp(4.592 v_{\text{disc}}^{\max}/v_{\text{obs}}^{\max}), \quad (25)$$

which has been converted to $(v_{\text{disc}}^{\max}, z_0)$ and is plotted as the dashed line in Fig. 11. Extrapolation to $v_{\text{disc}}^{\max} = 180$ km s⁻¹ indicates that a stable disc for that case should be achieved approximately near $h/z_0 = 3.1$ or $z_0 = 1450$ pc, which represents a puffed up disc rarely seen in reality (van der Kruit & Searle 1982; Kregel et al. 2002).

Obviously, this criterion is derived for one specific galactic constitution and its general, dimensionless applicability should be further assessed. Does it hold, for example, for a different v_{obs}^{\max} ? An indication that it indeed holds comes from the study of Bottema & Gerritsen (1997) where a similar stability change over has been established for a disc with $v_{\text{obs}}^{\max} = 120$ km s⁻¹. The applicability of Eq. (25) will diminish when the galaxy is appreciably different from the late type spiral studied in this paper. For example if the disc deviates from exponential, when there is a substantial bulge, or when the gas content is much larger. It is not expected that medium differences in gas content will play an important role because as we already saw, the bar develops just as well with or without gas. A more general discussion, mainly relating to other stability criteria will be given in Sect. 9.

As described above, before the bar develops the disc exhibits some strong spiral features. These features are transient and as a consequence the disc heats up, possibly aided by additional scattering on gas accumulations or clouds. When a bar is present the surrounding disc is heated by emanating arms of variable strength. This heating leads to an increased disc thickness which is indicated by the arrows towards larger z_0 values in Fig. 11. As can be seen, when a disc is more unstable the heating and thickening is larger, a result which does not come as a surprise. Noteworthy is the fact that in general when the disc becomes thicker it remains approximately equally thick at all radii. This even holds for the barred region where the thickness is rigorously calculated as the azimuthally averaged rms z-height and using $z_0 = 1.10 z_{\text{rms}}$. Only when a bulge develops from gas transported inwards the thickness remains small or even becomes smaller in the bulge region.

6.4 Dead or alive

The present simulations are performed with a rigid, “dead”, bulge and dark halo potential. What might change when instead, the bulge and halo would be composed of a collection of particles? To answer this question one has to distinguish between two aspects:

- A) Bar formation and
- B) Bar persistence

Let’s first consider item A. In first instance the development of the bar depends on the potential of the halo and bulge. A more massive halo or bulge increases the potential energy and stabilizes against bar formation. For the bulge there is an additional effect. When the bulge becomes more massive an ILR is forced by the higher circular speed near the centre which frustrates the bar formation (Toomre 1981; Sellwood & Evans 2001). These effects are the result of a deeper, azimuthally symmetric, potential well and consequently changing from a dead to a life mass distribution

will not alter the formation of the bar and the stability criterion of Eq. (25) remains valid. In second instance, however, during the process of bar formation there might be a difference if the halo and/or bulge were alive. A life component allows angular momentum transfer more easily and resonances between disc and halo might occur. Because the maximum disc case ($v_{\text{disc}}^{\text{max}} = 180 \text{ km s}^{-1}$) has a relatively light halo it is feasible to perform a numerical calculation with a life dark halo composed of not too massive particles. This has actually been done, using 70k halo plus bulge, 70k disc, and 16k gas particles. The result is nearly identical to the case with a rigid halo and bulge as presented in the bottom row of Fig. 8, both during and at the end of the simulation after 1.5 Gyrs. This proves that for at least this situation a dynamical interaction between an emerging bar with a surrounding life component is not important.

Bar persistence (item B) is a different story. When an already barred galaxy is embedded in a life, non rotating isotropic dark halo, the bar is slowed down by dynamical friction (Debattista & Sellwood 1998). Eventually the bar will then dissolve. This slowing down is severe when the galaxy is considerably sub maximum and is nearly absent when close to a maximum disc situation. The initial situation of Debattista & Sellwood is, of course, rather specific and in reality a dark halo will acquire some rotation during galaxy formation (Tremaine & Ostriker 1999). According as a halo rotates faster, the dynamical friction process is less severe and so in reality the bar dissolution will be less strong than Debattista & Sellwood claim. Nevertheless, if the simulations were to be performed with a life halo there would be a dynamical influence on the persistence of the bar. Fortunately, as demonstrated above, bars which develop in a more sub maximum disc situation tend to be smaller. Such bars then reside in a region where the disc density is still larger than the dark halo density. Consequently the slowing down mechanism will only be slightly active if the halo were life. The mechanism of Debattista & Sellwood is important for sub maximum discs with large bars, a situation that maybe never occurs in reality.

A life bulge may, just as a life halo, also influence the persistence of an already existing bar by dynamical friction. In addition one might imagine that a small bulge becomes aligned with the bar, enforcing its presence. Concerning bulges, it should be kept in mind that the investigated galaxy has only a small bulge; the surface density of the bulge is larger than that of the disc for radii less than 0.9 kpc. The bars which develop are generally much larger than that extent, and any effect of a life bulge on the bar is therefore minor. For an earlier type galaxy with larger bulge the situation might be different.

It would be, nevertheless, interesting to investigate numerically the effects of a life bulge and halo on the persistence of the bar. But that is less simple than it might seem. At first, realistic and preferably slightly rotating halos and bulges have to be created. Secondly, halos are massive and large numbers of particles have to be used. If, instead, one replaces the halo (and bulge) with less and more massive particles inevitably stochastic heating of the bar and surrounding disc will occur. The bar then dissolves by a numerical effect and drawing conclusions is difficult.

7 THE STATE OF THE GAS

7.1 Rain-clouds

A good assessment of the state of the gas can be obtained by plotting the position for every SPH particle in a temperature – density diagram. Two of such diagnostic plots are shown in Fig. 12 for two exemplary cases: $v_{\text{disc}}^{\text{max}} = 126 \text{ km s}^{-1}$ with $z_0 = 675 \text{ pc}$ and $v_{\text{disc}}^{\text{max}} = 165 \text{ km s}^{-1}$ with $z_0 = 900 \text{ pc}$. In all the simulations a typical “rain-cloud” structure develops. Most of the gas resides around 10^4 K which is the equilibrium between FUV heating and the practical upper limit set to the temperature by the cooling function. In circumstances of high density and/or low FUV flux gas may cool and starts to rain down from the cloud. The solid line indicates the Jeans instability threshold. If a gas particle falls below this line and remains there for a period greater than t_{span} , half its mass is converted into a stellar particle and the other half into a hot SN particle. This rain-cloud structure represents a rather uneasy and dynamical equilibrium state. If, for example, the FUV flux is removed, nearly all the gas falls to low temperatures within two time steps. Only at low densities gas may remain warm by the CR heating. Not shown in the diagnostic plot is the hot SN gas. This gas has a temperature around $1.25 \cdot 10^7 \text{ K}$ (for $\epsilon_{\text{SN}} = 25\%$) and densities in the range of 0.002 to $0.2 \text{ M}_{\odot} \text{ pc}^{-3}$. If the hot SN phase is switched off the gas particles generally move back to the 10^4 K phase very quickly. When a bar develops, as for $v_{\text{disc}}^{\text{max}} = 165 \text{ km s}^{-1}$ (bottom panel of Fig. 12) a typical extension on the 10^4 K cloud towards high density appears. In such cases inwards transport of gas generates numerous young stars of which the heating outweighs the intrinsic cooling.

Four temperature ranges have been defined: cold for $T < 1000 \text{ K}$, luke warm for $1000 \text{ K} < T < 8000 \text{ K}$, warm for $8000 \text{ K} < T < 10^5 \text{ K}$, and hot (SN) for $T > 10^5 \text{ K}$. For the top panel in Fig. 12 with $v_{\text{disc}}^{\text{max}} = 126 \text{ km s}^{-1}$ the total amount of gas is $18.7 \cdot 10^9 \text{ M}_{\odot}$ of which $13.1 \cdot 10^9 \text{ M}_{\odot}$ resides in the stellar disc region, where $R < 25 \text{ kpc}$. Of this amount, 18.5%, 25.9%, 54.8%, and 0.9% is in the cold, luke warm, warm, and hot phase respectively. In case of $v_{\text{disc}}^{\text{max}} = 165 \text{ km s}^{-1}$, given in the bottom panel of Fig. 12 the total amount of gas is $17.9 \cdot 10^9 \text{ M}_{\odot}$ of which $12.1 \cdot 10^9 \text{ M}_{\odot}$ is at $R < 25 \text{ kpc}$. Division of that last amount into the cold to hot phases gives fractions of 15.8%, 20.6%, 62.6%, and 1.1%.

There is a considerable amount of luke warm gas; in most cases even more than the amount of cold gas. Even if one were to increase the cold fraction by increasing the f_c parameter (Eq. 8) then still the same amount of luke warm gas remains. This fact is caused by the abovementioned uneasy and dynamical equilibrium state of the gas. SPH particles are continuously dropping out of the rain-cloud by natural cooling and are pushed up there again by heating. In a manner, this contradicts the proposed notion of a two phase ISM (Field et al. 1969) or three phase ISM (McKee & Ostriker 1977). Although artificially implemented the hot SN state of the gas can be considered as the hot phase of this three phase ISM model.

7.2 The ratio of cold to warm H I

The whole process of cloud collapse, division in smaller fractions, further collapse, star formation, bubble formation, etc,

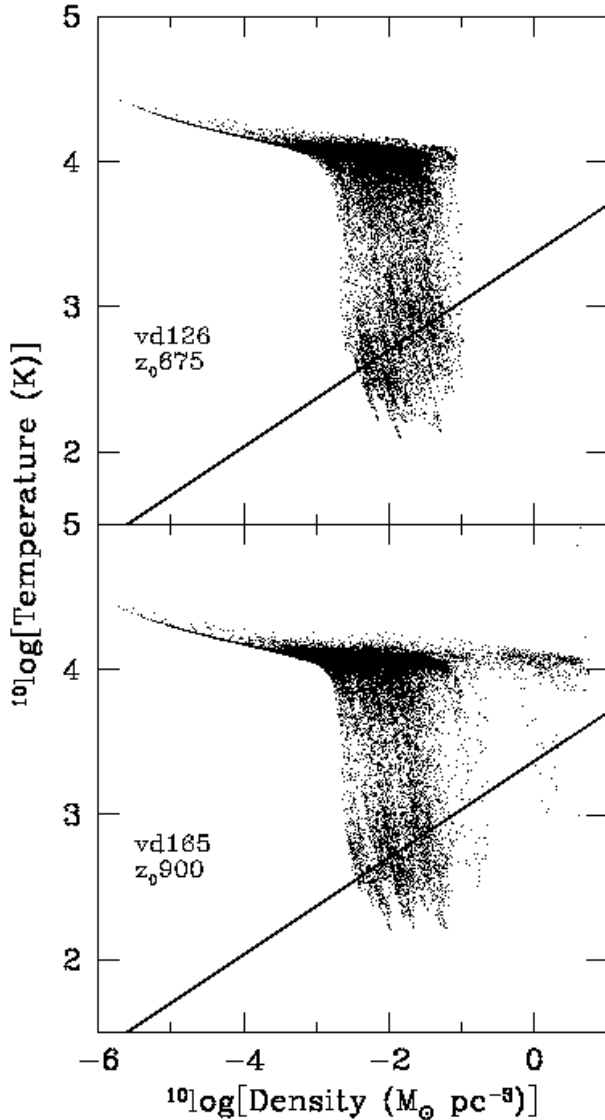


Figure 12. Temperature versus density of the gas for two typical simulations; $v_{\text{disc}}^{\text{max}} = 126 \text{ km s}^{-1}$ with $z_0 = 675 \text{ pc}$ (top panel) and $v_{\text{disc}}^{\text{max}} = 165 \text{ km s}^{-1}$ with $z_0 = 900 \text{ pc}$ (bottom panel). Each dot represents one gas (SPH) particle. The structure is an equilibrium between intrinsic cooling and heating by the FUV field. Once a gas particle falls below the Jeans instability line (full drawn line) and remains there for a certain time span, it will form a stellar particle. The extension at 10^4 K towards high density in the bottom panel is typical for gas inside a bar.

is extremely complex and not well understood. But anyway, if at a region gas cools and starts to collapse it takes a certain amount of time for the first stars to appear. In the present simulations this is implemented by requiring a certain time span t_{span} (Eq. 8) the gas has to remain Jeans unstable and thus cold before it may form stars. The longer t_{span} , the more cold gas is present and one would like to fix this parameter by comparing simulated warm to cold gas ratios with actually observed ratios in spiral galaxies. Moreover, the effect of the amount of SN feedback appears to be slightly related to the amount of cold gas and so related to t_{span} .

Unfortunately, observations to determine this ratio are

difficult and the ensuing analysis is ambiguous. In our local Galactic neighbourhood it seems that cold and warm H I are evenly divided (Kulkarni & Heiles 1987, Payne et al. 1983), though there appears to be luke warm gas (Kalberla et al. 1985) as well, which considerably complicates the analysis. For external galaxies the presence of cold gas has been established (Braun 1997, Young & Lo 1996) yet the amount is undetermined. Comparing galaxies, Dickey & Brinks (1993) demonstrate that the ratio of cold to warm gas may differ considerably from system to system yet its absolute value depends on the unknown temperature (or temperature range) of the cold gas. Finally I came to conclude that, as for now, the observations allow a fraction of cold H I gas anywhere between 15 and 80%. This is all rather disappointing and means that not much more can be done than quoting gas ratios for the various simulations.

There are, nevertheless, two interesting facts predicted by the simulations. At first the presence of a sizable amount of luke warm gas. Secondly, a large cold H I gas fraction leads to excessive clumping and giant SF regions. If the ratio of cold to warm H I does appear to be large in an actual galaxy, an additional stabilization mechanism is needed for the cold gas. In this respect magnetic fields might be a good candidate.

7.3 H I , H₂, and dust

An important result of the research by Kennicutt (1989) is that the Schmidt law holds for the total ($\text{H}_2 + \text{H I}$) gas surface density. This means that the H_2 in the inner regions of galaxies actively participates in generating instabilities and the ensuing star formation. As for most late type galaxies, also in the inner regions of NGC 628 there is a gradual increase of the $\text{H}_2/\text{H I}$ ratio (see Fig. 2). Following the result of Kennicutt, the total gas should and has been included in the simulations. But there is a problem. H_2 is in a dense region where according to the Schmidt law there is a lot of SF and consequently a high FUV field. That field should quickly dissociate the existing H_2 . In real galaxies this does not happen and thus another process is needed to maintain the H_2 which is not incorporated in the simulations.

Above a certain density threshold the atomic gas becomes molecular. This threshold depends on the pressure, the radiation field, and metals plus dust. Especially dust is needed to shield the molecules from photodestruction (Elmegreen 1993). In addition dust allows H_2 to form on grain surfaces (Hollenbach & Salpeter 1971). Therefore dust explains, at least for a large part, why H_2 can exist in the presence of the high FUV field. But this also means that at positions with large H_2 column densities there has to be more dust than at other positions. This is in agreement with the finding of Huizinga & van Albada (1992) that absorption in galaxies mainly takes place in the inner regions.

Remains the problem that in the simulations the H_2 is simply replaced with additional H I gas. As noted in the beginning of this subsection, that has to be done to be able to follow the Schmidt law. Yet at the central regions of a real galaxy heating and cooling might proceed differently compared to the H I mechanism. It will likely proceed at lower temperature regimes and FUV flux will be attenuated by the extra dust. Nevertheless one does not expect heating and cooling to be substantially different because the

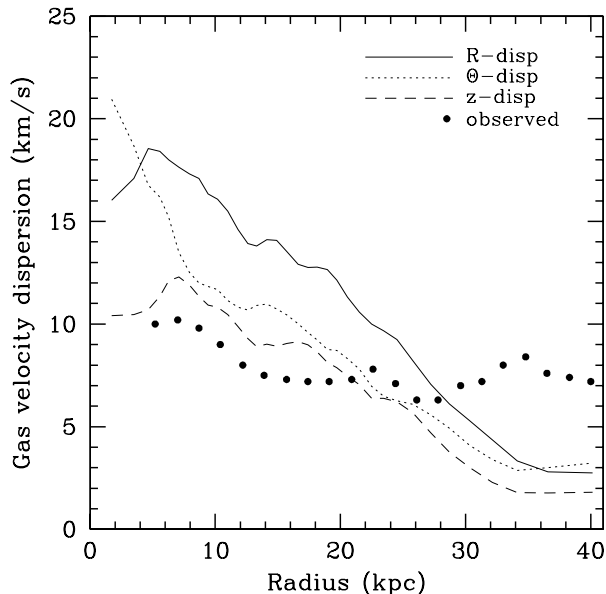


Figure 13. Velocity dispersion of the gas in the three spatial directions as a function of radius after 1.5 Gyrs of simulation. The dots give the observed z-velocity dispersion in NGC 628 which is, inside the stellar disc region ($R < 25$ kpc), in good agreement with the simulated values.

same metal ions responsible for the cooling (C^+ and O^{++}) are present. Compared to dynamical time scales SF is fast and in a practical numerical sense always takes place in a few timesteps. Considering this, and the presence of only a moderate amount of H_2 (8.5%), it seems reasonable that the replacement of H_2 by $H I$ in the simulations will not result in errors on scales larger than the employed spatial and time resolution.

7.4 The velocity dispersion of the gas

If there is no SN feedback but only FUV heating the resulting gas velocity dispersion is in the range of 4 to 7 km s^{-1} in the stellar disc region. When SNs are included the gas can be stirred up to higher dispersions as was noted by Gertsen (1997). For a simulation with $v_{\text{disc}}^{\text{max}} = 126 \text{ km s}^{-1}$, $z_0 = 675 \text{ pc}$ using 40k gas particles (see next section) the resulting velocity dispersion at $t = 1.5 \cdot 10^9$ years is plotted in Fig. 13. By the way, for 16k gas particles the result is identical. One can see in Fig. 13 that the velocity dispersion decreases when going to larger radii. This is caused by less star formation taking place further out in the disc and consequently there is less SN action, being less able to stir up the gas. What is interesting is that the radial velocity dispersion is significantly larger than the dispersion in the other directions, similar to the stellar velocity dispersions. The actually observed gas z-velocity dispersion in NGC 628 (Kamphuis 1993, van der Hulst 1996) is also given in Fig. 13. There is a good agreement between the observations and simulations, which suggests that the employed mechanism of SN feedback quite accurately simulates the processes taking place in reality.

Actually matters are more complicated than suggested in the paragraph above. At first because the hydrodynamics

is approximated by a finite resolution numerical scheme. Secondly because the $H I$ gas in a real galaxy is not a continuous medium, but a hierarchical ensemble of clouds. This ensemble of clouds cannot be considered as a fluid in equilibrium. The clouds and thus the $H I$ can be heated by gravitational scattering. In that case a velocity dispersion is predicted of 5 to 7 km s^{-1} independent of cloud mass (Jog & Ostriker 1988, Gammie et al. 1991). Additional heating can, of course, take place through kinetic energy input by SNs. It is unclear if, and how accurately the numerical scheme is able to describe the detailed process of heating for an ensemble of clouds. An indication that there is indeed such a shortcoming is the simulated low dispersion values at radii beyond 30 kpc: 2 to 3 km s^{-1} is simulated while 5 to 7 km s^{-1} is predicted and observed. Obviously the simulated gas is not discrete enough or too viscous.

8 SPIRAL STRUCTURE

8.1 40k gas simulations

In order to make a more detailed analysis of spiral structure it appeared beneficial to increase the number of gas particles from 16.000 to 40.000, giving a gas mass per SPH particle of $4.7 \cdot 10^5 M_{\odot}$. Simulations with the increased number of gas particles show lots more details and structure. To illustrate this, in Fig. 14 the resulting structure is displayed for four cases which have been investigated for various reasons. The top two rows are for a galaxy with maximum disc rotation of 126 km s^{-1} , $z_0 = 675 \text{ pc}$, $\epsilon_{\text{SN}} = 25\%$ and adding $4 M_{\odot} \text{ yr}^{-1}$ of new gas. Fig. 15a is after a simulation time of 1.5 Gyrs and, except for the larger particle number, is equal to the situation in Fig. 5c. Comparing the two one can notice that especially in the inner regions more gas particles gives a more pronounced spiral structure. In the outer regions the spiral arms are more continuous, less flocculent, and contain fewer star formation spots. Overall, the general appearance of the mass and gas distribution and of the spiral structure has not changed by using more gas particles. This implies that medium and large scale structures which are generated do not depend on the employed particle number. A quantitative analysis of structures can thus be made and the result should be generally valid.

In Fig. 14b the simulation of Fig. 14a has been continued until 3 Gyrs to investigate disc heating and the effect of an increased young population of stars. The lower two rows of Fig. 14 are for a galaxy with maximum disc rotation of 150 km s^{-1} , $z_0 = 900 \text{ pc}$ (14c) and $z_0 = 675 \text{ pc}$ (14d) at $t = 1.5$ Gyrs. These two simulations are on opposite sides of the bar instability threshold for that maximum disc rotation. Fig. 14c is, except for the larger particle number, equal to Fig. 8b and the same conclusions apply as for the comparison of the $v_{\text{disc}}^{\text{max}} = 126 \text{ km s}^{-1}$ discs, given above.

8.2 Stellar heating

A long simulation of a stable disc provided the possibility to investigate the evolution of the stellar velocity dispersion. New stars are formed at a rate of approximately $4 M_{\odot} \text{ yr}^{-1}$ with an original velocity dispersion equal to that of the gas.

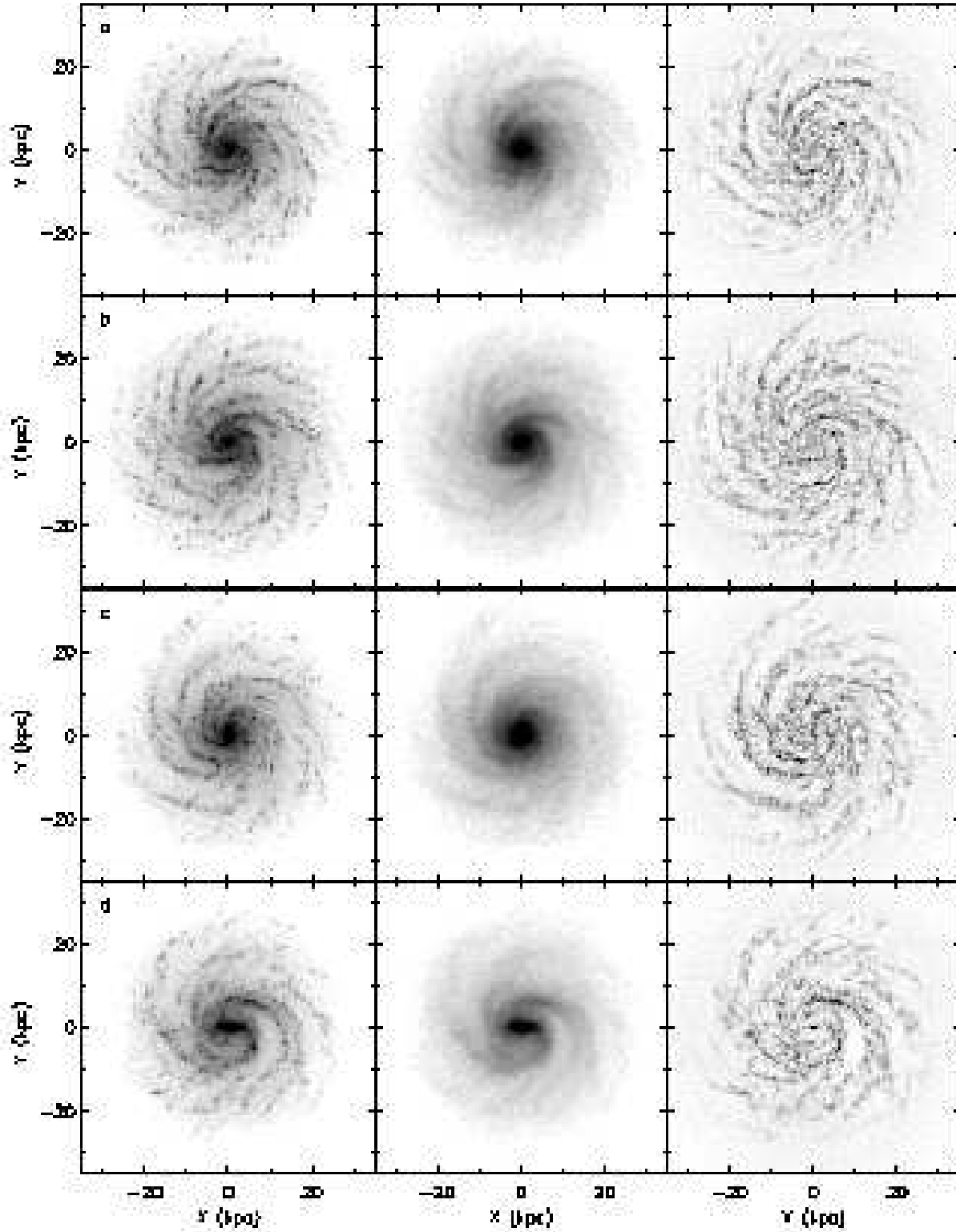


Figure 14. **a to d** The resulting structure of the galaxy using 40k gas and 150k stellar particles. **a** For $v_{\text{disc}}^{\text{max}} = 126 \text{ km s}^{-1}$, $z_0 = 675 \text{ pc}$, at $t = 1.5 \text{ Gyrs}$. **b** As **a** but now at $t = 3 \text{ Gyrs}$. **c** For $v_{\text{disc}}^{\text{max}} = 150 \text{ km s}^{-1}$, $z_0 = 900 \text{ pc}$ at $t = 1.5 \text{ Gyrs}$. **d** As **c** but for $z_0 = 675 \text{ pc}$. More gas particles increases the resolution which results in a more detailed spiral structure specially in the inner regions.

Over a time span of a few Gyrs these young stars will acquire an ever larger velocity dispersion.

The proven stable disc with $v_{\text{disc}}^{\text{max}} = 126 \text{ km s}^{-1}$ and $z_0 = 675 \text{ pc}$ was simulated for 3 Gyrs using 150k stellar, and 40k gas particles. For the whole period gas was added to the system at a rate of $4 M_{\odot} \text{ yr}^{-1}$ to compensate for the gas consumption by star formation. At $t = 3 \text{ Gyrs}$, the situation displayed in Fig. 14b, the then available stars were divided in five age groups. The youngest stars have an age $< 0.75 \text{ Gyrs}$, there are three groups with ages between 0.75 to 1.5 Gyrs, 1.5 to 2.25 Gyrs, and 2.25 to 3 Gyrs, and there is a group of old stars present from the onset of the simulation, thus having an age $> 3 \text{ Gyrs}$. At radii of 5, 10, 15, and 20 kpc the velocity dispersion in both the radial and vertical direction was determined of these age groups. The result is given as a function of the square root of the age of each group in Fig. 15. In this way the evolution of the dispersion can be monitored at each radial position. As can be seen, the increase in dispersion is nicely consistent with a square root of age functionality. After 3 Gyrs the dispersion of the old population has not yet been reached. If one extrapolates the data points to larger ages, then on average, after $\sim 6.5 \text{ Gyrs}$ the dispersion of the old, equilibrium population of stars will be reached.

An overview of the rates and the mechanisms of disc heating is given by Binney & Tremaine (1987, p. 470 - 484) and by Lacey (1991). In short, the collisionless stellar ensemble of a stellar disc can be heated by three principal mechanisms. Firstly, heating by molecular clouds (Spitzer & Schwarzschild 1953, Villumsen 1985), which generates heating $\propto t^{0.25}$. Secondly, heating by transient spiral features (Carlberg & Sellwood 1985) which is more efficient and heats $\propto t^{0.5}$ but molecular clouds are needed in addition to generate vertical heating. A third mechanism is heating by the infall of small satellite galaxies. Stellar heating as observed in the solar neighbourhood indicates that the heating, or increase in velocity dispersion, proceeds proportional to $t^{0.5}$ (Wielen 1977) so that the more effective spiral arm heating is needed to explain this observation.

The simulation of Fig. 14a and b actually includes, both heating by simulated molecular clouds (conglomerates of gas particles), and heating by transient spiral arms. It should therefore give a reasonable description of heating as occurring in real galactic discs. As witnessed in Fig. 15 the simulated heating is indeed consistent with a proportionality $\propto t^{0.5}$, as observed in our Galaxy and predicted by spiral arm heating. However, as mentioned in Sect. 4.4 the simulation is only collisionless for $R \lesssim 2h$. Therefore, for radii larger than $\sim 9 \text{ kpc}$ the simulations have additional heating by particle scattering. This will generate heating time scales being shorter than for real galaxies, certainly at the radial positions of 15 and 20 kpc.

8.3 On what does the amount of spiral structure depend?

My original perception concerning the creation of spiral structure was that its origin lies in an underlying young and cold stellar fraction. To investigate this assumption, for two stable discs ($v_{\text{disc}}^{\text{max}} = 126 \text{ km s}^{-1}$, $z_0 = 675 \text{ pc}$ and $v_{\text{disc}}^{\text{max}} = 150 \text{ km s}^{-1}$ with $z_0 = 900 \text{ pc}$) long simulations using 40k gas particles have been performed until $3 \cdot 10^9$ years. During this

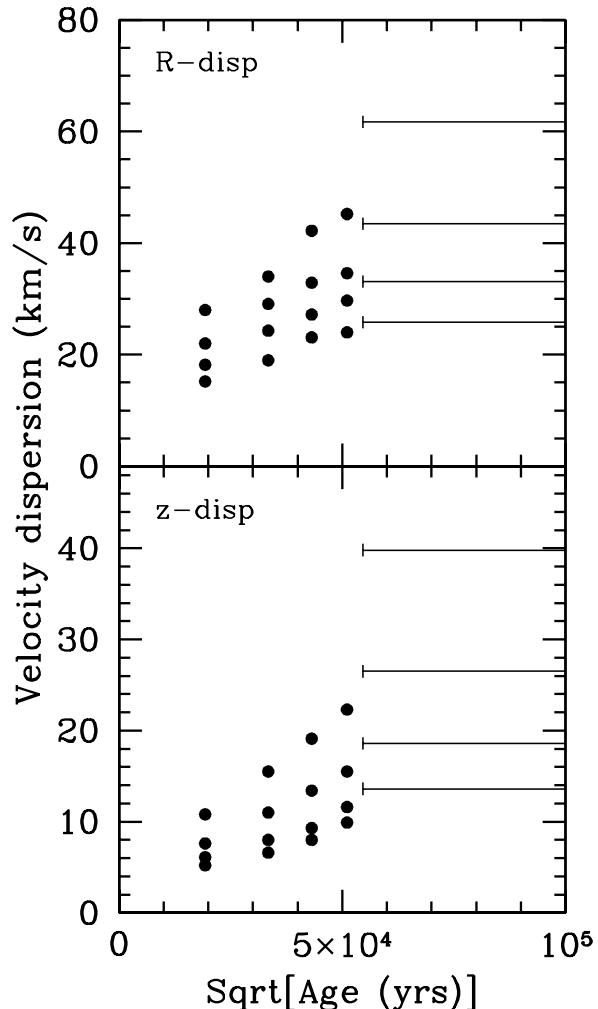


Figure 15. The time evolution of the stellar velocity dispersion in the radial direction (top) and vertical direction (bottom panel) derived from the simulation presented in Fig. 14b. Stellar particles are divided up into five age bins at four radial positions of 5, 10, 15, and 20 kpc. For each bin at each radius the dispersion is calculated. The old stars, present from the onset of the simulation (age $> 3 \text{ Gyrs}$) are indicated by the bars. At each age bin a larger dispersion is for a smaller radius. It appears that the stellar heating is consistent with being proportional to $t^{0.5}$.

time young stars have been created at a rate of $\sim 4 M_{\odot} \text{ yr}^{-1}$ at the position and with the kinematics of the gas layer. The result was disappointing. As can be seen in Fig. 14a and b, the spiral structure might be marginally stronger at 3 Gyrs compared to that after 1.5 Gyrs. However, if the whole time sequence for this $v_{\text{disc}}^{\text{max}} = 126 \text{ km s}^{-1}$ run is inspected then there are no gradual changes any more after $\sim 1 \text{ Gyrs}$. There are fluctuations in the appearance and strength of the spiral arms over periods of $\sim 0.2 \text{ Gyrs}$ which is illustrated as the difference between Fig. 14a and Fig. 14b. The same conclusion applies for the $v_{\text{disc}}^{\text{max}} = 150 \text{ km s}^{-1}$, $z_0 = 900 \text{ pc}$ case (Fig. 14c). If the addition of gas is stopped after 1.5 Gyrs, the SFR decreases to $\sim 2 M_{\odot} \text{ yr}^{-1}$ at $t = 3 \text{ Gyrs}$ and the spiral structure slowly fades away.

In retrospect this failure of a young population to gen-

erate a more pronounced spiral structure can be understood. For example, the $v_{\text{disc}}^{\text{max}} = 126 \text{ km s}^{-1}$ disc has a total stellar mass of $45.5 \cdot 10^9 M_{\odot}$. During the simulations cold stars are added at a rate of $4 M_{\odot} \text{ yr}^{-1}$. After 1 Gyrs the cold stellar fraction then amounts to $4 \cdot 10^9 M_{\odot}$, and after 3 Gyrs to $12 \cdot 10^9 M_{\odot}$ which is approximately 20% of the then available total stellar mass. However, the stars which were formed first are then not young and cold any more because of stellar heating. As can be seen in Fig. 15, after 3 Gyrs, the stars with that age have increased their velocity dispersion to more than half of that of the old population. Considering the numbers and heating rates, the mass fraction of a reasonably cold stellar population will not surpass the amount of 20%. Such a fraction might locally destabilize the disc to some extent but will never become a dominant mechanism.

The total mass of a disc with $v_{\text{disc}}^{\text{max}} = 150 \text{ km s}^{-1}$ is $64.5 \cdot 10^9 M_{\odot}$. In that case for a SFR of $4 M_{\odot} \text{ yr}^{-1}$ the mass fraction of cold stars is approximately 10%, being a factor two smaller than for the $v_{\text{disc}}^{\text{max}} = 126 \text{ km s}^{-1}$ disc. For a more massive disc, with the same gas content it would thus be even more difficult to create instabilities by the cold stellar population process, and vice versa, of course. Some additional experiments have been carried out by adding large quantities of gas during the beginning of the simulations. As a result the SFR goes up and a larger cold stellar fraction is generated. The spiral structure then becomes more pronounced, but subsides to its usual state once the extra gas flow is stopped. In these cases it is not clear whether the more pronounced spiral structure is generated by the larger cold stellar fraction or by the larger amount of gas which is present.

Since an increased cold stellar fraction barely enhances the spiral structure, the influence of other parameters has been investigated. It was apparent from the investigation of Sect. 5 that spiral structure is mainly caused by shearing gas structures and an increased fraction of cold gas might enhance such a process. For the situation of Fig. 14c, $v_{\text{disc}}^{\text{max}} = 150 \text{ km s}^{-1}$ and $z_0 = 900 \text{ pc}$, the collapse factor f_c (Eq. 8) has been increased by a factor four in combination with or without a change of the supernova efficiency. A larger collapse factor produces more cold gas, which is colder and has densities up to a factor of 10 larger. The gas arms are thinner and more threadlike and tend to form gas clumps which cause strong star formation regions. For a combination of $t_{\text{span}} = 2 \times t_{\text{ff}}$ and a low SN efficiency of $\varepsilon_{\text{SN}} = 10\%$ the image is like the top rows of Fig. 5 and not like any actual galaxy. Consequently, the attempt to make more massive gas concentrations by increasing the cold gas fraction and lowering the SN dispersal mechanism is successful, but produces the familiar clumps and does not enhance a global spiral pattern. Letting ε_{SN} remain at 25% or making it larger in combination with a larger cold gas fraction does generate the more threadlike gas structure, but does not create larger or significantly smaller spiral disturbances in the underlying stellar density structure. What this investigation makes clear is that the generated spiral structure as it is in Fig. 14c is only weakly dependent on the exact value of the gas parameters. Putting it in other words, a significant change of cold gas fraction or supernova efficiency does not lead to large changes in the spiral structure morphology.

The standard cooling function applied to the situation of NGC 628 leads to a slightly large value of the observable

SFR, when compared with what is actually observed. Such a large SFR had the advantage of quickly generating an appreciable amount of young and cold stars of which the effect on the emerging spiral structure could be investigated. Since such effects are demonstrated to be minor, the cooling function can be changed so as to generate a lower SFR. This has been investigated for the present case ($v_{\text{disc}}^{\text{max}} = 150 \text{ km s}^{-1}$, $z_0 = 900 \text{ pc}$) by lowering the SFR to $\sim 2\frac{1}{2} M_{\odot} \text{ yr}^{-1}$ and adding only $2 M_{\odot} \text{ yr}^{-1}$ of gas constantly. It appears that there are no noticeable differences in the generated spiral structure compared to a situation with a larger SFR. From this follows that spiral structure at low gas suppletion rates can be sustained longer if the cooling of the gas is less efficient.

One can conclude that small and medium scale spiral structure as displayed in Fig. 14a to c can be generated in an isolated spiral disc, for a large range of gas parameters. The principle factor determining the strength of the spiral structure is the surface density of the gaslayer. However, it is not possible to create autonomously a large scale spiral density wave. If the disc is thinner and colder and crosses the threshold of bar instability the bar can then drive an $m = 2$ spiral structure as demonstrated in Fig. 14d.

8.4 A quantitative analysis of spiral structure

One would like to compare the spiral structure produced by the simulations with the actual spiral structure in real galaxies in some quantitative way. For example, the number of spiral arms, their shape, and strength. Astonishingly only a small amount of research has been carried out in this respect and a comparison of simulations with observations is only marginally possible.

The shapes of spiral arms are generally well represented by a logarithmic functionality (Danver 1942, Kenicutt 1981) as

$$r = r_0 e^{\tan(i_p) \Theta}, \quad (26)$$

where r is the position on the arms with belonging angle Θ and i_p is the pitch angle. Rewriting Eq. (26) gives $\ln(r) \propto \tan(i_p) \Theta$. When the density structure of a (face-on) galaxy is rebinned to a $(\ln(r), \Theta)$ plane, logarithmic spirals show up as straight lines. Derivation of the pitch angles for each arm is straightforward and the number of crossings of one feature over the 2π long Θ axis gives the m -mode of the feature. On various occasions simulations have been displayed in such a plane and the simulated arms are always well represented by a logarithmic shape. However, $(\ln(r), \Theta)$ planes are not easily comparable because there is in fact too much and too dispersed information. One would like to reduce the information into less and more informative numbers.

One method to do this has been explored by Considère & Athanassoula (1982, 1988). It involves a Fourier transform of the image of the galaxy into a superposition of global m -armed logarithmic spirals following Kalnajs (1975). A two dimensional grid (i, j) is transformed into Fourier coefficients $A(p, m)$ by

$$A(p, m) = \frac{\sum_i \sum_j w_{ij} \exp[-i(p \ln(r_{ij}) + m \Theta_{ij})]}{\sum_i \sum_j w_{ij}}, \quad (27)$$

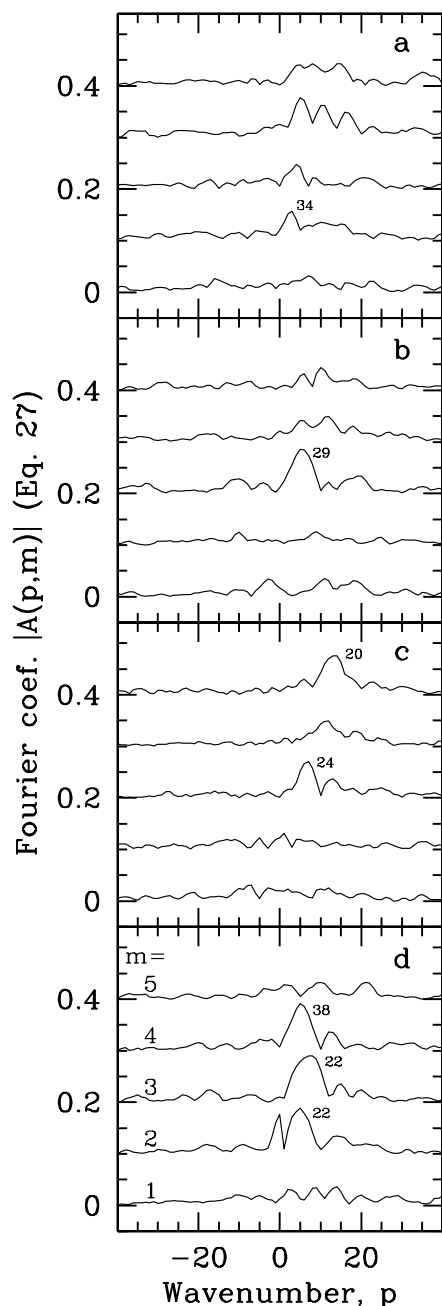


Figure 16. **a to d** Amplitude of the Fourier coefficients $A(p, m)$ of the V-band images in Fig. 14a to d using global logarithmic spirals as base function (Eq. 27). For each panel the lines from bottom to top are for $m = 1$ to 5 and are offset by 0.1 with respect to each other. The belonging pitch angle is indicated by the numbers for a few features. At panel **d** the signal at $p = 0, m = 2$ originates from the bar of Fig. 14d.

where p is the wavenumber, m the mode and w_{ij} the value at gridpoint i, j . The pitch angle i_p is given by $\tan(i_p) = -m/p$ at the wavenumber where $|A(p, m)|$ has its largest amplitude. Considère & Athanassoula (1988) present the calculated Fourier coefficients in their Fig. 5 for 16 spiral galaxies, among which are a number known to have a well developed grand design structure. For most of the galaxies the coefficients $|A(p, m)|$ rarely surpass the level of 0.1. Notable

exceptions are NGC 5247 ($|A(p, m = 2)| \sim 0.45$) and NGC 6946 ($|A(p, m = 2)| \sim 0.21$), but these two galaxies both have exceptionally large pitch angles of 26 and 32° respectively. Considère & Athanassoula claim that the two-armed component is everywhere dominant, but a close inspection of their data shows that only for 8 out of 16 galaxies $m = 2$ is dominant, while for 6 out of 16 the $m = 1$ component dominates! Surely this indicates that a number of systems have undergone some kind of interaction. NGC 628 is in the sample and shows a maximum $|A(p, m = 2)|$ of 0.16 with a pitch angle of 16°. In addition there is a peak for $m = 3$ at a level of 0.09 with pitch angle of 28°.

For the V-band images of the simulated galaxies in Fig. 14 the Fourier coefficients for modes one to five have been calculated following Eq. (27) and are displayed in Fig. 16. In general the peak values do not exceed the level of 0.1, as for most of the real galaxies, in fact. Fig. 16 is only one snapshot; if the Fourier coefficients are monitored over a time span, peaks come and go for modes 2 to 5. Time scales are typically 0.2 Gyrs and levels are comparable to those displayed in Fig. 16a to c. This behaviour reflects the episodic nature of the small and medium scale spiral structure during the simulations. For Fig. 16d, the barred galaxy, peaks are more constantly present. The simulations are supposed to represent NGC 628. As can be seen in Fig. 16, the values of the Fourier coefficients do not reach the observed value. In addition, simulated pitch angles are somewhat too large. Although the simulated V-band images reasonably resemble images of actual galaxies, the observed image of NGC 628 (for example on page 99 of the Shapley-Ames catalog, Sandage & Tammann 1981) shows arms which are longer and less open. This means that the real galaxy NGC 628 exhibits more a grand design than its simulated counterpart. A further discussion of this matter will follow in Sect. 10.

As determined by Kennicutt (1981), pitch angles of late type galaxies lie in the range between 12 and 30° and have a median value of 18°. As such, the pitch angles of the simulated galaxies are slightly large but certainly not unusual. Note that for the galaxies in common to the samples of Considère & Athanassoula and Kennicutt the derived pitch angles are in good agreement. But this brings me to the question: how representative are both these samples for an average galaxy? Probably not representative at all. For both samples, galaxies are selected at least partly, for having a grand design or otherwise well delineated spiral structure. Inevitably this produces a severe bias towards high amplitude spiral signal and probably towards smaller pitch angles.

An alternative way to analyse spiral structure has been employed by a.o. Elmegreen et al. (1989, 1992), Rix & Zaritsky (1995), and Fuchs & Möllenhoff (1999). According to this method, first the underlying smooth galactic distribution is removed. Then the residual is divided up in a number of circular annuli of which the brightness B is Fourier analysed with respect to the azimuthal angle ϕ :

$$B = \sum_1^{10} c_m \cos(m(\phi - \phi_m)). \quad (28)$$

Following Fuchs & Möllenhoff the coefficients c_m will be displayed as a function of radius to obtain a direct and quantitative insight into the development of the multiplicity of the structure. A determination of the pitch angle of mode m

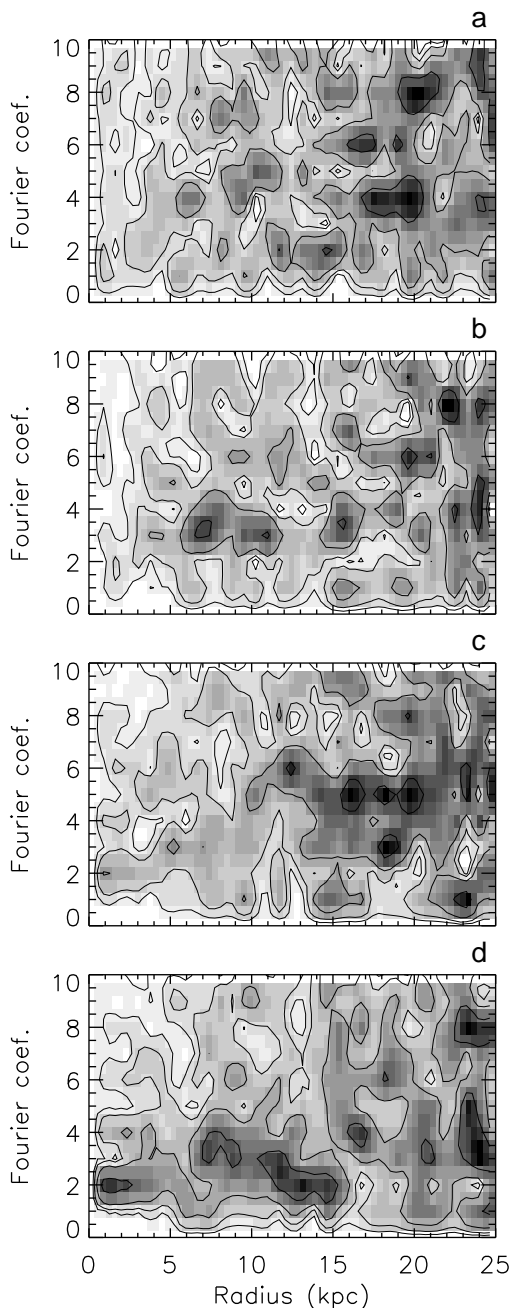


Figure 17. Amplitude of the coefficients of the Fourier sum along circular annuli as a function of radius for the four V-band images of Fig. 14a to d. Contour levels are at 5, 10, 20, 40, and 80% of the underlying smooth galactic brightness level. Specific features can easily be related to features in Fig. 14 and Fig. 16.

might be done by plotting the phase ϕ_m versus $\ln(\text{radius})$, but this has not been investigated presently.

The V-band images of Fig. 14 have been divided up into 35 equally wide annuli ranging from a radius of 0.5 to 25 kpc. After division by the continuum, the Fourier coefficients of Eq. (28) were calculated and are displayed in Fig. 17. One may notice that a good impression can be obtained of the radial functionality of the multiplicity of the spiral structure. Comparing Fig. 16 and Fig. 17, certain features

can be related and put at its proper radius. For example, in panel **a** the small $m = 2$ signal originates from radii between 11 and 15 kpc, while the $m = 4$ signal comes mainly from positions in the outer regions. In panel **b** the $m = 3$ spiral with pitch angle of 29° can obviously be recognized in Fig. 17. On the other hand, the small $m = 2$ signal in panel **c** of Fig. 17 at radii < 3 kpc cannot readily be seen in Fig. 16c. Such a feature appears small in relative units, but if this disturbance of $\sim 15\%$ is expressed in absolute values for NGC 628 it amounts to $\sim 25 L_\odot \text{pc}^{-2}$, which is certainly not negligible. Expressed in relative units, Fig. 17 shows that the brightness fluctuations become larger at larger radii. In absolute units, however, the signal dominates in the inner regions. For the barred galaxy in panel **d** it can be noticed that the $m = 2$ inner bar drives the $m = 2$ spiral arms further out, except for the small excursion to $m = 3 - 4$ around a radius of 8 kpc. Of course, during the simulation the spiral structure changes and consequently also its representation as given in Fig. 17.

Though this is a nice way to display the spiral structure of a galaxy, there is a major problem. There are hardly any observations which have been interpreted in this manner and hence a comparison between simulations and real data is not really possible. Rix & Zaritsky (1995) give c_1 to c_6 values for K' -band observations of 18 face-on spirals. Their main intent was to investigate the lopsidedness of galaxies and thus they focussed on the c_1 coefficient. The near infrared data do not extend beyond three scalelengths and the values of the c_3 to c_6 coefficients over that radial extent are relatively small, yet consistent with the values in Fig. 17. Only Fuchs & Möllenhoff (1999) give a detailed Fourier coefficient analysis for one galaxy: NGC 1288. Both, the values and radial functionality of the coefficients show a striking similarity with the simulations of non-barred galaxies. NGC 1288 is a regular, massive galaxy with clear spiral structure but has no grand design density wave permeating its disc. As such it is comparable with the simulations and the spiral structure shows a comparable morphology.

9 SWING AMPLIFICATION

The spiral structure which develops in the present numerical simulations of an isolated and bar stable galaxy appears to be generated by swing amplification. This phenomenon where small distortions can be severely amplified in a differentially rotating (shearing) disc was discovered by Goldreich & Lynden-Bell (1965) and the theory has been elaborated by o.a. Julian & Toomre (1966), Toomre (1981), Athanassoula (1984), and Athanassoula et al. (1987). As noted by Toomre (1981) swing amplification is governed by a conspiracy between three processes: shear, shaking and self-gravity. Each of these processes can be specified by a dimensionless parameter: Γ , Q , and X which are the shear rate, the familiar Toomre's Q parameter and as it is sometimes called Toomre's X parameter. In principle, swing amplification has been derived and quantified for a one component, infinitely thin disc using the epicyclic approximation. That is a simplification of reality which should be kept in mind when comparing results of the theory with findings for a real or numerical galaxy.

To investigate whether swing amplification is indeed the

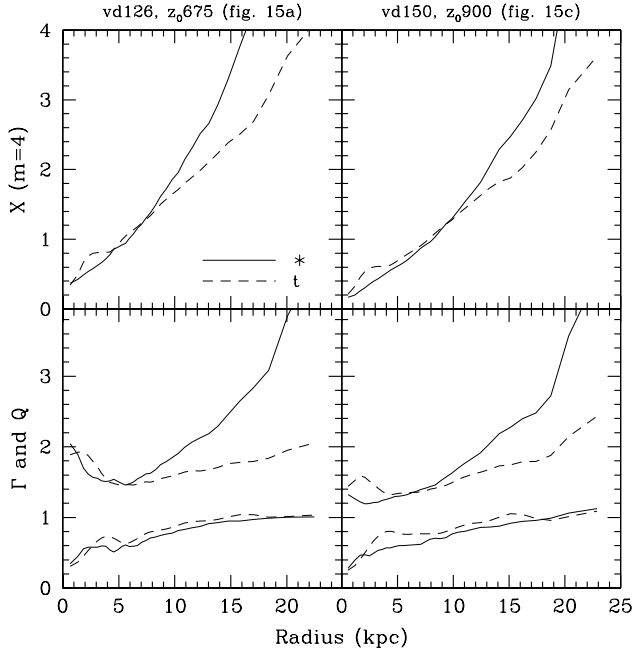


Figure 18. Swing amplification parameters $X(m=4)$, Γ , and Q as a function of radius for the galaxies of Fig. 14a and Fig. 14c. These parameters are defined in two ways (*: Eq. 22+29+31, t : Eq. 23+30+32) depending on the way the influence of the gas is included.

cause of the numerical spiral structure, the theory has been applied to the galaxies displayed in Fig. 14. The three above-mentioned parameters have to be calculated for the galactic constitution which leads again to the problem encountered in Sect. 6.2 of what to substitute for the rotation and surface density. As in Sect. 6.2 where two kinds of Q are defined also here two kinds of Γ and X will be defined; pure stellar (Γ_* and X_*) given by

$$\Gamma_* = -\frac{R}{\Omega_*} \frac{d\Omega_*}{dR}, \quad (29)$$

$$X_* = \frac{\kappa_*^2 R}{2\pi G m \sigma_*}, \quad (30)$$

and total or testparticle parameters (Γ_t and X_t) given by

$$\Gamma_t = -\frac{R}{\Omega_{\text{gas}}} \frac{d\Omega_{\text{gas}}}{dR}, \quad (31)$$

$$X_t = \frac{\kappa_{\text{gas}}^2 R}{2\pi G m (\sigma_* + \sigma_{\text{gas}})}. \quad (32)$$

Here Ω and κ are the orbital and epicyclic frequencies, σ is the surface density and m is the azimuthal multiplicity of the disturbance which is equal to the number of spiral arms. For the galaxies of Fig. 14a ($v_{\text{disc}}^{\text{max}} = 126 \text{ km s}^{-1}$, $z_0 = 675 \text{ pc}$, $t = 1.5 \text{ Gyrs}$) and Fig. 14c ($v_{\text{disc}}^{\text{max}} = 150 \text{ km s}^{-1}$, $z_0 = 900 \text{ pc}$, $t = 1.5 \text{ Gyrs}$) the swing amplification parameters are given as a function of radius in Fig. 18. As can be seen, there is only a marginal difference between Γ_* and Γ_t . On the other hand, the Q and X parameter may differ substantially mainly depending on whether the gas surface density is, or is not included.

Athanassoula (1984) has calculated the maximum am-

plifications for a number of different values of the three dimensionless parameters. By interpolating her Fig. 26, the amplification can thus be found. But this is a maximum amplification provided the arrival phase of the distortion is optimum. This means that for an actual case the amplification may be less, or zero, or the amplification of a distortion which emerges at a later time with more optimum arrival phase may approach this maximum limit. When viewed over a longer time span the spiral pattern will thus be rather variable just as witnessed in the simulations. Inspection of Athanassoula's Fig. 26 establishes some generalities, though. For a Γ value between 0.5 and 1.0 swing amplification is only effective for X between typically 0.5 and 2.5 and has the largest amplifications when X lies between 1.0 and 1.5. A large value of Q dampens the amplification; when $Q \gtrsim 2.0$ the amplification is $\lesssim 3$. When Q is low, say $Q \lesssim 1.2$ then the amplifications may exceed the value of 30.

For the present two galaxies of which the parameters are displayed in Fig. 18 the maximum amplifications have been derived as a function of radius. To that aim the pure stellar (*) and total (t) curves have simply been averaged using the assumption that the gas layer and its gravitation will influence the swing amplification process to some extent. If the amplifications would have been derived for both curves separately the emerging picture would not be essentially different. This is because an increasing Q value results in a decreasing amplification with a factor barely dependent on Γ and X . A difference between the X curves mainly appears at large values of X where the amplification is small anyway. The maximum amplifications for modes 2, 3, 4, 6, and 12 are displayed as a function of radius in Fig. 19.

One may notice that the smaller m -modes ($m=2, 3$) or the two and three armed spiral structures allow the largest amplification at the smaller radii. Spiral structures with more arms will preferentially develop further out. At certain radii the amplifications for a number of different modes can approximately be equally large. In practice that means that the number of arms will, and likely will, change from time to time. For the less massive disc ($v_{\text{disc}}^{\text{max}} = 126 \text{ km s}^{-1}$, top panel of Fig. 19) the amplifications reach at most a factor of four which is mainly caused by the relatively large value of Q . When that simulation is continued to 3 Gyrs as displayed in Fig. 14b the swing amplification parameters barely change. Consequently also the amplifications appropriate for that later time are equal to those already given for $t = 1.5 \text{ Gyrs}$. If the disc is more massive (bottom panel of Fig. 19), Q is smaller and the allowed amplifications are larger certainly for the smaller m -modes. For the same disc but with a smaller thickness ($z_0 = 675 \text{ pc}$ instead of 900 pc) as in Fig. 14d the resulting Q parameter (at $t = 0$) is smaller while the X and Γ parameters remain nearly equal. The emerging amplification scheme for that thinner disc is then equal to that in the bottom panel of Fig. 19 except that all the amplifications have to be multiplied with a factor $2\frac{1}{2}$ to 3. That results in values between 30 and 40 for $m=2, 3$, and 4 at radii $< 10 \text{ kpc}$. But, as we know a bar develops in that case which might be related to these allowed large amplifications. When one compares the amplifications given in Fig. 19 with the actually emerging modes in Fig. 17 one may note the exceptional correspondence. For example, the $m=3$ structure in Fig. 17b between 6 and 11 kpc and the same allowed mode by swing amplification at exactly

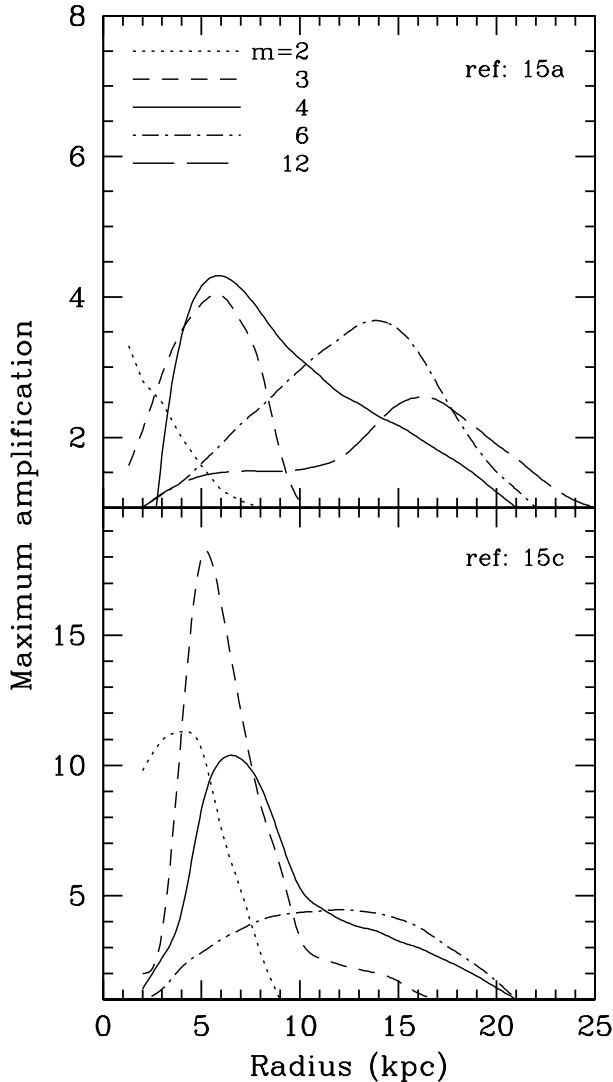


Figure 19. The maximum amplification factors given by swing amplification theory for the galaxies of Fig. 14a (top) and Fig. 14c (bottom). Note that at certain radii the amplifier may be active and equally strong for different arm multiplicities.

the same radii. Even nicer is the correspondence between Fig. 17c and Fig. 19 bottom panel. In that case the radial functionality of the appearing structure and the predicted amplifications are in striking agreement.

To investigate if the magnitude of the disturbances is consistent with swing amplification theory, for the case of Fig. 14c the initial gas distortions have been compared with the eventual strength of the stellar mass arms. For example at $R = 3$ kpc gas mass fluctuations are $\sim 3.5 M_{\odot} \text{pc}^{-2}$ and the $m = 2$ stellar mass arms have a strength of $\sim 23.6 M_{\odot} \text{pc}^{-2}$ implying an amplification of a factor ~ 6.7 . The allowed maximum amplification of $m = 2$ at $R = 3$ kpc is ~ 11 , in perfect agreement with the simulations. Likewise, at $R = 5$ kpc for $m = 3$ one has an amplification of ~ 4.7 while a maximum of ~ 17 is allowed, and at $R = 13$ kpc amplifications are ~ 2.2 while ~ 4.5 is allowed.

One may conclude that the predictions of swing amplification theory and the results of the numerical simulations

are completely consistent. Not only for the radial positions where the modes preferentially occur, but also for the actual strength of the spiral arms.

10 DISCUSSION AND CONCLUSIONS

10.1 On grand design

For a late type bar stable galaxy in isolation it does not seem possible to have a grand design spiral density wave pervading its disc. The spiral structure which does develop is on a medium and small scale with a multiplicity increasing as a function of radius. That finding can be explained qualitatively and quantitatively by swing amplification; a process which occurs naturally in a differentially rotating disc. If swing amplification can explain the structure for a late type galaxy so well, it is likely that it also applies for other, more earlier types. The question which then emerges is whether for some galaxy swing amplification allows a spiral structure with a constant multiplicity over a sizable range of radii. Such a situation would, in principle, be equal to a grand design.

To answer the question one could calculate the amplification factors for a number of observed galaxies and investigate if a certain mode is dominant over a large radial extent. Such a calculation has been done by Athanassoula et al. (1987) but unfortunately they do not present the radial modal functionality. A global insight can be obtained by considering equations 29 and 30 and Fig. 18. To make a constant radial multiplicity, the Γ parameter can only be slightly variable and the X parameter needs to be nearly constant. For NGC 628 (Fig. 18) that is certainly not the case. Making a constant X requires that $\kappa^2 R / \sigma$ is constant, while in the mean time the rotation curve should be rather flat. That results in the condition that $\sigma R \sim \text{constant}$ which is impossible to achieve for an exponential disc ($\sigma \propto e^{-R/h}$). It can, however, not be excluded that for some rotation curve and photometry a constant X over an extent of, say, two scalelengths can be achieved.

For a number of well known grand design galaxies the $m = 2$ mode is the dominant one. How can such a situation arise when swing amplification is the driving mechanism? For a late type galaxy (like NGC 628) figures 18 and 19 can again give some insight. In case of a maximum disc rotation of 126 km s^{-1} (and $z_0 = 675 \text{ pc}$) the amplifications are given in the top panel of Fig. 19. For radii between 3 to 10 kpc the $m = 4$ mode is the largest. Inspection of Eq. (30) shows that exactly the same X values are achieved when half the multiplicity (m) is used and a double value of the surface density. Then Fig. 19 (top) has also the same appearance but the $m = 4$ is replaced with $m = 2$, while the amplifications are much larger because Q is smaller. As a consequence $m = 2$ is dominant between 3 and 10 kpc and might drive a grand design $m = 2$ through the rest of the galaxy. The problem is, however, that the surface density has to be doubled, which makes the disc massive, with a maximum rotation of $\sim 180 \text{ km s}^{-1}$ and then a bar emerges. So, as soon as a late type galaxy reaches the state that $m = 2$ is active over a considerable radial extent and with enough amplitude, its disc is so massive that instead a bar develops. This explains the results of the numerical calculations in this paper, namely

that only multiple, non grand design spirals appear, or a bar when the disc is more massive. Unless, of course, one explicitly prevents the development of a bar (Elmegreen & Thomasson 1993). Then a grand design $m = 2$ may exist in a hypothetical galaxy.

For late type galaxies it seems impossible to create a grand design and for other disc like galaxies it seems to be very difficult. How does nature then make the well known beautiful spiral galaxies which adorn so many front pages of astronomy books? What can at first be noticed is that these beautiful galaxies all belong to a very small and select group; there are simply not many of such galaxies. What can further be noticed is that these galaxies generally have companions. Kormendy & Norman (1979) already remarked that: “in general a galaxy shows a global spiral pattern ... by having a density wave driving mechanism in the form of a bar or a companion”. For example, well known grand designs with clear signs of interaction are: M81, M51, M101, NGC 7753, NGC 5364, and NGC 4305. An interaction with accompanying tidal forcing gives, in principle, a natural explanation for an emanating $m = 2$ symmetry. In addition both theoretical and numerical calculations (Toomre 1981) show that even a modest external forcing may produce a transient grand design spiral pattern. Such a pattern when viewed from the right angle looks very similar to the observed morphological and kinematical structure of, for example, M81 (Visser 1980). Considering these arguments and the present numerical simulations of isolated galaxies, I then conclude that nearly all non barred grand design spirals are created by an interaction.

But how about NGC 628? That galaxy is supposed to be the template for a typical late type galaxy, yet its observed spiral structure is more of a grand design nature than can be generated in the simulations. This apparent contradiction can be resolved by looking at the neutral hydrogen observations of NGC 628 (Kamphuis & Briggs 1992) which show that NGC 628 is not that isolated after all. Instead two gas clouds with masses of $\sim 10^8 M_\odot$ are situated on opposite sides of the centre at a radius of $\sim 12'$. In fact the image of these clouds in Fig. 3 of Kamphuis & Briggs is similar to the gravitational forcing displayed in Fig. 1 of Toomre (1981). That modest forcing already generates a huge transient spiral wave in the underlying galactic disc. Although the exact forcing of the gas clouds in NGC 628 is not known, these clouds can certainly explain the grand design structure of NGC 628 by swing amplification.

10.2 On the mass contribution of the disc

When the stellar velocity dispersion of a disc is measured the possibilities for a galaxy’s internal constitution are severely restrained. For a locally isothermal disc one has the relation

$$v_{\text{disc}}^{\text{max}} = 0.88 \langle v_z^2 \rangle_{R=0}^{1/2} \sqrt{\frac{h}{z_0}}, \quad (33)$$

Bottema (1993). This equation can be rewritten to $z_0 \propto (v_{\text{disc}}^{\text{max}})^{-2}$ and can be drawn onto Fig. 11 once the scale-length and dispersion ($\langle v_z^2 \rangle_{R=0}^{1/2}$) are measured. For example, lets take NGC 628 being clearly not barred, which restricts the galaxy to lie in the stable section of Fig. 11. Unfortunately the stellar velocity dispersion is not measured, but

can be inferred from Fig. 3 of Bottema (1993) such that $\langle v_z^2 \rangle_{R=0}^{1/2} = 60 \pm 10 \text{ km s}^{-1}$. For a scalelength of 4.5 kpc, Eq. (33) when related to Fig. 11 implies that $v_{\text{disc}}^{\text{max}} < 150 \text{ km s}^{-1}$, even though the thickness of the disc is not known. A more massive disc would bring the galaxy into the bar unstable region, obviously not consistent with its appearance.

A different approach to determine the contribution of the disc has been employed by Athanassoula et al. (1987). They use swing amplification theory to investigate the presence of the amplifier for a certain mode in case of different disc contributions. For a sample of 48 galaxies with reasonably accurate rotation curves this investigation has been performed. It appears that, in order to avoid $m = 1$, for the majority of the sample implies that the disc is less massive than the so called “maximum disc situation, having a halo without a hollow core”. In practice that means $v_{\text{disc}}^{\text{max}}/v_{\text{obs}}^{\text{max}} \approx 0.9$. The threshold for allowing $m = 2$ is for the majority of the sample at an M/L ratio approximately half of that to avoid $m = 1$ (not surprisingly). In terms of rotational values one then has no $m = 2$ amplification any more for $v_{\text{disc}}^{\text{max}}/v_{\text{obs}}^{\text{max}} < \frac{1}{2}\sqrt{2} \times 0.9 = 0.64$. That are the facts presented by Athanassoula et al. A problem is, however, that it is unclear what is meant with “requiring that the amplifier is active”. Is a minimum amplification required? And over what radial extent is it required to be active? For instance can Fig. 19 be regarded as presenting an active $m = 2$ mode?

A second problem is associated with the interpretation. For example the requirement of no $m = 1$ is in contradiction with the results of the Fourier analysis of Considère & Athanassoula (1988), which shows that for a large fraction of galaxies $m = 1$ is present and even dominant. On the other hand it is not known which fraction of real galaxies indeed has $m = 2$ dominant over a certain radial extent. Certainly there are a number of galaxies which do not have $m = 2$ present; which are flocculent or amorphous, which implies that $v_{\text{disc}}^{\text{max}}/v_{\text{obs}}^{\text{max}} < 0.64$ for that category. By using the swing amplification theory it is assumed that galaxies are not interacting, such that all $m = 2$ activity has an internal origin. That is certainly not valid and a number of galaxies could be featureless when they would be isolated.

Considering the facts presented by Athanassoula et al. and the discussion just presented, in my opinion, the observed range of morphologies of galaxies is certainly consistent with the average (non barred) galaxy having $v_{\text{disc}}^{\text{max}}/v_{\text{obs}}^{\text{max}} = 0.64$.

10.3 On bars

In Eq. (25) a dimensionless bar stability criterion is given for a galaxy comparable to NGC 628. The criterion depends on two parameters: $v_{\text{disc}}^{\text{max}}/v_{\text{obs}}^{\text{max}}$ and the aspect ratio z_0/h . Here I shall elaborate on other parameters that may be of influence for a more general galaxy, but shall not go into details on bar formation (see e.g. Lynden-Bell 1979; Toomre 1981; Binney & Tremaine 1987, p 381).

Earlier type galaxies have more prominent bulges. Adding a bulge to a disc plus halo situation has two effects. Firstly, the rotation curve is made flatter in the inner regions, creating an ILR. Such an ILR may frustrate or inhibit the formation of a bar. Secondly adding a bulge means that the disc is dynamically less important and the

bulge may be considered as a kind of substitute halo. The combination of both effects results in a galaxy being more stable against bar formation if its bulge is more massive. An extreme example of this is presented by Sellwood & Evans (2001) where they replace in the inner regions nearly the complete dark halo by a bulge. The maximum disc rotational contribution is then 75% and the minimum Q value amounts to 1.75. That galaxy is stable, which is not surprising when one considers the rotational contributions and Q values presented in Sect. 6.

The bar forms just as well with or without the amount of gas typical for an Sc galaxy. This is contrary to the claim by Shlosman & Noguchi (1993) that a considerable gas content may inhibit the formation of a bar. Their calculations, however, do not include star formation and consequently no SF feedback. As a result a few “superclouds” develop which rapidly spiral inwards by dynamical friction and strongly heat up the stellar content in the inner regions. The galaxy is then too hot to form a bar. In reality star formation sets in and under normal conditions such massive gas clouds will never form.

Different bar stability criteria have been derived before. At first, for example, the T/W criterion by Ostriker & Peebles (1973). That criterion is derived for MacLaurin spheroids and is as such only applicable for that kind of theoretical galaxy. Furthermore, the T and W are not easily related to observable quantities. What the calculations of Ostriker & Peebles did make very clear was that a large spherical (dark) matter contribution is an effective way to stabilize against bars.

A second bar stability criterion put forward by a.o. Sellwood & Carlberg (1984) is the requirement of a specified minimum Q value. The problem is to actually determine that Q value. As demonstrated in Sect. 6, Q is not unique, certainly not when gas is present in a disc. Moreover Q has a radial functionality which will be different when the radial mass profile is different. One then has to consider the minimum Q value, or require Q to be below a certain value over a certain radial extent. Even then a small difference in Q can mark the change over from stable to unstable. What can be determined from the investigations in this paper is that stability problems arise as soon as Q (Q_* or Q_t) at some radius falls below the value of ~ 1.2 . It may, however, also be 1.1 or 1.3 if the constitution of the galaxy is slightly different.

A third criterion is the one by Efstathiou et al. (1982) stating that a disc is stable to bar formation if

$$\frac{v_{\text{obs}}^{\text{max}}}{\sqrt{GM_{\text{disc}}/h}} \gtrsim 1.1. \quad (34)$$

This criterion can be rewritten considering that for an exponential disc $\sqrt{GM_{\text{disc}}/h} = 1.61v_{\text{disc}}^{\text{max}}$ such that Eq. (34) translates into $v_{\text{disc}}^{\text{max}}/v_{\text{obs}}^{\text{max}} \lesssim 0.56$ in order to be stable. Considering Fig. 11 which contains the criterion of the present study, it is clear that Efstathiou et al.’s criterion is overly restrictive. In addition, for very thin discs with $h/z_0 \gtrsim 12$ it is not valid, though such thin discs are probably not present in reality.

10.4 Outlook

It would be desirable to include the effects of dust and metals in the numerical code. Then matters like FUV shielding, variable cooling functions, and H_2 formation can be investigated. That might be important in cases like starburst galaxies or ULIRGs.

A grand design in a non-barred realistic galaxy still has to be created. Since that does not appear to be possible in an isolated galaxy, encounters have to be simulated. Small satellites passing a large galaxy can be simulated using a dead halo, but for larger satellites dynamical friction becomes important and a life halo must be used. Re-creation of the M51 encounter or the M81-M82 interaction would be a nice challenge.

An obvious extension of the present work is to investigate bar stability for galaxies with more massive bulges. A three parameter stability criterion might then be derived.

It appears difficult to compare numerical spiral structure with actual spiral structure in a quantitative way. This is mainly caused by the lack of observational data on spiral structure. Surely a program to obtain such data is not that difficult. Moreover, asymmetries in galaxies can then be investigated by determination of the amount of $m = 1$ and from that the presence and frequency of interactions might be established.

10.5 Conclusions

Finally a compilation of the main conclusions following from the numerical simulations and the subsequent analysis and considerations.

(i) A disc in star formation equilibrium is established by two opposing actions. On the one hand gas cooling and dissipation, on the other hand gas heating by the FUV field of young stars and mechanical SN feedback.

(ii) Too little SN feedback results in a disc with giant SF regions; too much SN feedback disperses the gas and dilutes the spiral structure.

(iii) Spiral features are generated in the disc by shearing gas filaments which swing amplify the underlying mass distribution.

(iv) Spiral arms exist for approximately half a rotation period and disappear by winding and stretching or by interaction with other spiral features.

(v) A confirmation is given of Ostriker & Peebles (1973) result that a late type spiral galaxy is more unstable to bar formation when its disc contribution to the total mass is larger.

(vi) A late type spiral galaxy is more unstable to bar formation when its thickness or equivalently its stellar velocity dispersion is lower.

(vii) A bar stability criterion is determined for late type galaxies, depending on the ratio of maximum disc rotation to total rotation and on disc thickness.

(viii) The bar stability of a disc barely depends on the amount of gas.

(ix) At the maximum disc limit a bar stable galaxy can only be created for a disc which is unrealistically thick.

(x) The simulations display the presence of a substantial (20 – 25%) amount of luke warm H I gas in the temperature range from 1000 to 8000 K.

(xi) In the stellar disc the simulated velocity dispersion of the gas is in good agreement with the observations.

(xii) The increase of the stellar velocity dispersion (stellar heating) of newly formed stars proceeds proportional to $t^{0.5}$, as observed in the solar neighbourhood. After ~ 6.5 Gyrs the velocity dispersion level of the old stellar population is reached.

(xiii) The simulations generate small and medium scale spiral structure of which the multiplicity increases as a function of radius.

(xiv) It is not possible to create a grand design $m = 2$ spiral. Unless a bar develops which may drive the $m = 2$ structure.

(xv) When compared with some exemplary spiral galaxies, the numerically generated spiral structure is less strong and has a larger multiplicity.

(xvi) The emerging spiral structure is qualitatively and quantitatively consistent with the theory of swing amplification.

(xvii) Swing amplification explains that for a late type galaxy a dominant $m = 2$ mode over a considerable radial extent can only exist in a massive disc. Such a disc is unstable to bar formation. As a consequence a grand design $m = 2$ spiral cannot develop in an isolated bar stable late type galaxy, just as predicted by the numerical simulations.

(xviii) The suggestion of Kormendy & Norman (1979) is confirmed that most of the grand design $m = 2$ spirals must be generated by an interaction or are driven by a central bar.

(xix) The observed range of morphologies of galaxies is consistent with the average (non barred) galaxy having $v_{\text{disc}}^{\text{max}}/v_{\text{obs}}^{\text{max}} = 0.64$.

Acknowledgments

I thank J. Gerritsen for donating his numerical package to me, for introducing me to its use, and for many discussions. L. Hernquist is acknowledged for making his TREESPH code available to the astronomical community. I thank W. de Blok, R. Braun, and I. Pelupessy for useful discussions. The Kapteyn Institute is acknowledged for providing hospitality and support.

REFERENCES

- Athanassoula E., 1984, *Phys. Rep.*, 114, 319
Athanassoula E., 1992, *MNRAS* 259, 345
Athanassoula E., Bosma A., Papaioannou S., 1987, *A&A* 179, 23
Barbanis B., Woltjer L., 1967, *ApJ* 150, 461
Barnes J.E., Hernquist L., 1991, *ApJ* 370, L65
Barnes J.E., Hut P., 1986, *Nature* 324, 466
Bertin G., Romeo A.B., 1988, *A&A* 195, 105
Binney J., Tremaine S., 1987, *Galactic Dynamics*, Princeton Univ. Press, Princeton, NJ
Black J.H., 1987, in: *Interstellar Processes*, Hollenbach D.J., Thronson H.A. (eds), Reidel, Dordrecht, p. 731
Bodenheimer P., 1992, in: *Star Formation in Stellar Systems*, Tenorio-Tagle G., Prieto M., Sánchez F. (eds), Cambridge University Press, p. 3
Bottema R., 1993, *A&A* 275, 16
Bottema R., 1996, *A&A* 306, 345
Bottema R., 1997, *A&A* 328, 517
Bottema R., Gerritsen J.P.E., 1997, *MNRAS* 290, 585
Braun R., 1995, *A&AS* 114, 409
Braun R., 1997, *ApJ* 484, 637
Bruzual B.A., Charlot S., 1993, *ApJ* 405, 538
Casertano S., 1983, *MNRAS* 203, 735
Carlberg R.G., Sellwood J.A., 1985, *ApJ* 292, 79
Combes F., Becquaert J.-F., 1997, *A&A* 326, 554
Considère S., Athanassoula E., 1982, *A&A* 111, 28
Considère S., Athanassoula E., 1988, *A&AS* 76, 365
Courteau S., Rix H.W., 1999, *ApJ* 513, 561
Cox D.P., 1990, in: *The Interstellar Medium in Galaxies*, Thronson H.A., Shull J.M. (eds), Kluwer, Dordrecht, p. 181
Dalgarno A., McCray R., 1972, *ARA&A* 10, 375
Danver C.G., 1942, *Lund Obs. Ann.* 10
Debattista V.P., Sellwood J.A., 1998, *ApJ* 493, L5
de Jong, T., 1977, *A&A* 55, 137
Dickey J.M., Brinks E., 1993, *ApJ* 405, 153
Efstathiou G., Lake G., Negroponte J., 1982, *MNRAS* 199, 1069
Elmegreen B.G., 1993, *ApJ* 411, 170
Elmegreen B.G., 1992, in: *Star Formation in Stellar Systems*, Tenorio-Tagle G., Prieto M., Sánchez F. (eds), Cambridge University Press, p. 383
Elmegreen B.G., Thomasson M., 1993, *A&A* 272, 37
Elmegreen B.G., Elmegreen D.M., Seiden P., 1989, *ApJ* 343, 602
Elmegreen B.G., Elmegreen D.M., Montenegro L., 1992, *ApJS* 79, 37
Field G.B., Goldsmith D.W., Habing H.J., 1969, *ApJ* 155, L149
Freeman K.C., 1970, *ApJ* 160, 811
Friedli D., Benz W., 1993, *A&A* 268, 65
Friedli D., Benz W., 1995, *A&A* 301, 649
Fuchs B., Möllenhoff C., 1999, *A&A* 352, L36
Gammie C.F., Ostriker J.P., Jog C.J., 1991, *ApJ* 378, 565
Gerritsen J.P.E., 1997, Ph. D. Thesis, University of Groningen
Gerritsen J.P.E., de Blok J.W.G., 1999, *A&A* 342, 655
Gerritsen J.P.E., Icke V., 1997, *A&A* 325, 972 (GI97)
Gingold R.A., Monaghan J.J., 1977, *MNRAS* 181, 375
Goldreich P., Lynden-Bell D., 1965, *MNRAS* 130, 125
Habing H.J., 1968, *Bull. Astron. Inst. Netherlands* 19, 421
Heller C., Shlosman I., 1994, *ApJ* 424, 84
Hernquist L., 1987, *ApJS* 64, 715
Hernquist L., Katz N., 1989, *ApJS* 70, 419
Hollenbach D., Salpeter E.E., 1971, *ApJ* 163, 155
Huizinga J.E., van Albada T.S., 1992, *MNRAS* 254, 677
Jog C.J., Ostriker J.P., 1988, *ApJ* 328, 404
Julian W.H., Toomre A., 1966, *ApJ* 146, 810
Kalberla P.M.W., Schwarz U.J., Goss W.M., 1985, *A&A* 144, 27
Kalnajs A.J., 1975, in: *La dynamique des galaxies spirales*, Colloque International CNRS No. 241, Weliachew L. (ed), p. 103
Kamphuis J.J., 1993, Ph. D. Thesis, University of Groningen
Kamphuis J.J., Briggs F., 1992, *A&A* 253, 335
Katz N., 1992, *ApJ* 391, 502
Katz N., Gunn J.E., 1991, *ApJ* 377, 365
Kennicutt R.C., 1981, *AJ* 86, 1847
Kennicutt R.C., 1983, *ApJ* 272, 54
Kennicutt R.C., 1989, *ApJ* 344, 685
Kennicutt R.C., 1998, *ApJ* 498, 541
Kormendy J., Norman C.A., 1979, *ApJ* 233, 539
Kregel M., van der Kruit P.C., de Grijs R., 2002, *MNRAS* 334, 646
Kulkarni S.R., Heiles C., 1987, in: *Interstellar Processes*, Hollenbach D.J., Thronson H.A. (eds), Reidel, Dordrecht, p. 87
Lacey C., 1991, in: *Sundelius B. (ed), Dynamics of Disc Galaxies*, Dep. of Astronomy/Astrophysics, Göteborgs Univ. and Chalmers Univ. of Technology, Göteborg, p. 257
Lamers H.J.G.M.L., Leitherer C., 1993, *ApJ* 412, 771
Lin C.C., Shu F.H., 1964, *ApJ* 140, 646
Lin C.C., Shu F.H., 1966, *Proc. Nat. Acad. Sci.*, 55, 229
Lucy L.B., 1977, *AJ* 82, 1013
Lynden-Bell D., 1979, *MNRAS* 187, 101
Lynden-Bell D., Ostriker J.P., 1967, *MNRAS* 136, 293

- McCray R., Kafatos M., 1987, *ApJ* 317, 190
 McKee C.F., Ostriker J.P., 1977, *ApJ* 218, 148
 Mihos J.C., Hernquist L., 1994, *ApJ* 437, 611
 Mihos J.C., Hernquist L., 1996, *ApJ* 464, 641
 Monaghan J.J., 1989, *J. of Comp. Physics* 82, 1
 Mueller M.W., Arnett W.D., 1976, *ApJ* 210, 670
 Natali G., Pedichini F., Righini M., 1992, *A&A* 256, 79
 Navarro J.F., White S.D.M., 1993, *MNRAS* 265, 271
 Ostriker J.P., Peebles P.J.E., 1973, *ApJ* 186, 467
 Payne H.E., Salpeter E.E., Terzian Y., 1983, *ApJ* 272, 540
 Rix H.W., Zaritsky D., 1995, *ApJ* 447, 82
 Romeo A.B., 1994, *A&A* 286, 799
 Rubin V.C., Burstein D., Kent Ford W., Thonnard N., 1985, *ApJ* 289, 81
 Ryder S.D., Dopita M.A., 1994, *ApJ* 430, 142
 Salucci P., Ashman K.M., Persic M., 1991, *ApJ* 379, 89
 Sandage A., Tammann G.A., 1981, *A Revised Shapley-Ames Catalog of Bright Galaxies*, Carnegie Institute of Washington
 Schmidt M., 1959, *ApJ* 129, 243
 Sellwood J.A., Carlberg R.G., 1984, *ApJ* 282, 61
 Sellwood J.A., Evans N.W., 2001, *ApJ* 546, 176
 Sellwood J.A., Moore E.M., 1999, *ApJ* 510, 125
 Shlosman I., Noguchi M., 1993, *ApJ* 414, 474
 Shostak G.S., van der Kruit P.C., 1984, *A&A* 132, 20
 Shu F.H., Adams F.C., Lizano S., 1987, *ARA&A* 25, 23
 Silich S.A., Franco J., Palouš J., Tenorio-Tagle G., 1996, *ApJ* 468, 722
 Spitzer L., 1978, *Physical Processes in the Interstellar Medium*, Wiley & Sons, New York, p. 142
 Spitzer L., Schwarzschild M., 1953, *ApJ* 118, 106
 Springel V., 2000, *MNRAS* 312, 859
 Toomre A., 1964, *ApJ* 139, 1217
 Toomre A., 1981, in: *The Structure and Evolution of Normal Galaxies*, eds. Fall S.M. and Lynden-Bell D., Cambridge Univ. Press, Cambridge, p.111
 Tremaine S., Ostriker J.P., 1999, *MNRAS* 306, 662
 van Albada T.S., Sancisi R., 1986, *Phil. Trans. R. Soc. London, Ser. A*, 320, 447
 van der Hulst J.M., 1996, in: *The Minnesota lectures on extragalactic neutral hydrogen*, Astronomical Society of the Pacific Conference Series, Vol. 106, Skillman E.D. (ed), p. 47
 van der Kruit P.C., 1995, in: van der Kruit P.C., Gilmore G. (eds) *IAU Symposium No. 164, Stellar Populations*, Kluwer, Dordrecht, p. 205
 van der Kruit P.C., Searle L., 1981, *A&A* 95, 105
 van der Kruit P.C., Searle L., 1982, *A&A* 110, 61
 Villumsen J.V., 1985, *ApJ* 290, 75
 Visser H.C.D., 1980, *A&A* 88, 149
 Wevers B.M.H.R., van der Kruit P.C., Allen R.J., 1986, *A&AS* 66, 505
 Wielen R., 1977, *A&A* 60, 263
 Wolfire M.G., Hollenbach D., McKee C.F., et al., 1995, *ApJ* 443, 152
 Young L.M., Lo K.Y., 1996, *ApJ* 462, 203